Mechanical aspects of blood-wall interaction : wall shear stress measurement

Mechanical aspects of blood-wall interaction: wall shear stress measurement

F.J.H. Gijsen

WFW-report 95-149

CIP-DATA KONINKLIJKE BIBLIOTHEEK, DEN HAAG
Gijsen F.J.H.

Mechanical aspects of blood-wall interaction: wall shear stress measurement. F.J.H. Gijsen.
Eindhoven : Stan Ackermans Instituut.-I11.
WFW-report 95.149. -With ref.
ISBN 90-5282-556-4
Subject headings:
viscoelastic flow, wall shear stress measurement

ABSTRACT

The predilection of atherosclerotic lesions for specific sites in the arterial tree is believed to be related to the wall shear stress, exerted by the blood flow. Measurement of the magnitude of the wall shear stress is difficult and is frequently determined by an extrapolation of the velocity field to find the wall shear rate and an estimation of the viscosity of the fluid in the neighborhood of the wall. In this study, it will be shown that the non-Newtonian properties of blood significantly influence the velocity field and that the extrapolation of the near wall velocity distribution to determine the wall shear rate distribution is not very reliable. The estimation of the relevant viscosity of blood at near wall sites is not trivial due to its complex nature. Accurate measurement of the wall shear stress in this way is not feasible and a new method to evaluate the load of blood analog fluids on the wall will be presented.

Laser Doppler Anemometry measurements were performed in a three dimensional model of the human carotid artery bifurcation to investigate the influence of non-Newtonian fluid behavior. The blood analog fluid used in these experiments resembled the viscometric properties of blood quite closely. Velocity measurements under steady flow conditions ($Re = 300$) were performed for a Newtonian control fluid and the blood analog fluid. Both axial and secondary velocities were measured. Evident differences between the flow fields of the Newtonian and blood analog fluids were found. The non-Newtonian axial velocity field was flattened, had lower velocity gradients at the divider wall, and higher velocity gradients at the non-divider wall. The flow separation as found with the Newtonian fluid was absent, and secondary flow was strongly decreased. It was demonstrated that the extrapolation of the near wall velocity distribution to determine the wall shear rates is not very accurate and very sensitive to the estimated position of the wall. At the non-divider wall, the site where atherosclerotic lesions develop, the non-Newtonian properties of the blood analog fluid changed the sign of the wall shear rate and therefore the sign of the wall shear stress. It is therefore essential that the non-Newtonian properties of blood are included in a study that correlates the development of atherosclerotic lesions to local haemodynamics.

The inaccuracy of the wall shear rate measurements and the absence of a model to predict near wall viscosity instigated an investigation for a new method to measure the wall shear stress. If a highly flexible gel layer is attached to the inside of the model, the deformation of this gel layer is a measure for the wall shear stress. If the properties of the gel are known, the measured deformation of the gel layer can be converted to the wall shear stress. The small deformation of the gel layer was measured with Speckle Pattern Interferometry (SPI) and the performance of the newly developed SPI apparatus was evaluated in benchmark experiments. The wall shear stress was measured in a rectangular duct under steady flow conditions using a Newtonian measuring fluid. In a physiologically relevant range, the wall shear stresses were measured very accurately.

As a conclusion it can be stated that it is essential in *in-vitro* studies on atherogenesis that the non-Newtonian properties of blood are taken into account because they significantly influence the velocity distribution in physiologically relevant flow geometries. Furthermore, it is obvious that the existing methods of measuring the wall shear stress in *in-vitro* models are not satisfactory. A promising new method to measure the wall shear stress is presented and can be used to measure the mechanical load of blood analog fluid in *in-vitro* models.

Contents

Chapter 1

Introduction

Atherosclerosis is a complex disease that causes progressive occlusion of the lumen of arteries. From clinical practice it is known that specific sites in the arterial tree are sensitive to atherogenesis, the early stage of atherosclerosis. Local haemodynamics apparently play an important role in the development of atherosclerotic lesions. The predilection of atherosclerosis lesions for specific sites in the arterial tree is believed to be related to low or oscillating shear rates or shear stresses. Caro *et al.* (1971) developed a theory based on shear rate depended mass transfer mechanisms for small particles (e.g. cholesterol) suspended in the blood. The local shear rate governs the concentration distribution of these particles and thus the diffusion of these particles to the vessel wall. Combined with a model for the chemical reaction of the particles in the wall, they were able to link regions with low wall shear rates to the preferred sites for atherogenesis. Nerem (1992) argues that the endothelial cells are influenced by the local haemodynamics. The endothelial cells align with the flow direction and regions with low or oscillating wall shear stress might change the properties of the endothelial cells in a way that favors the process of atherogenesis. Both the study on the mechanical load of the endothelial cells induced by the blood flow and the near-wall rheology of blood in larger and medium sized arteries are of great interest.

Blood is a concentrated suspension of blood cells in plasma and its non-Newtonian properties are well established (Chien *et al.* (1969)). For the preparation of blood analog fluids as well as for the modeling of blood and blood flow, the composition and the properties of its main constituents have to be known and they will be discussed in section 2.2. From viscometric studies a constitutive equation for the fluid can be obtained, coupling the generated shear stresses to the imposed shear rates. In the viscometric devices, the fluid is assumed to be homogeneous and the shear rate constant. This assumption does not hold for blood and concentrated suspensions in general. The shear stress measurements in viscometric devices should therefore be combined with velocity and concentration measurements to enable prediction of the wall shear stress from the measured velocity gradient and concentration distribution in physiologically relevant flow systems. A review of available viscometric studies as well as concentration and velocity measurements in blood and blood analog fluids will be presented in section 2.3 and 2.4.

The local haemodynamics are not only governed by the pressure pulse and the geometry of the model but also by the fluid properties. The non-Newtonian properties of blood significantly alter the velocity distributions in small tubes, as can be concluded from chapter 2. For the study on the origin of atherosclerosis, it is important to investigate whether the non-Newtonian properties of blood influence the local haemodynamics in the larger and medium sized arteries. Experimental investigations on the influence of the non-Newtonian properties of blood in the larger arteries are relatively sparse (Liepsch and Moravec (1984)). In chapter 3, a blood analog fluid is presented that enables laser Doppler anemometry (LDA) measurements in a Plexiglass

model of the carotid bifurcation and the influence of the blood like properties of the fluid on the local haemodynamics and the wall shear rate are studied. Both axial and secondary velocities are measured and it will be shown that the viscoelastic properties of the blood analog fluid significantly influence the flow patterns in the carotid bifurcation. The estimated wall shear rates at the divider wall and the non-divider wall are compared.
The wall shear stress is defined as the product of the velocity gradient normal to the wall and the viscosity of the fluid at the wall. The wall shear stress values are usually determined by multiplying the wall shear rate, extrapolated from the measured velocity distribution, by the estimated viscosity. As can be concluded from chapter 2, the viscosity of blood near the wall can not be inferred directly from viscometric experiments. An accurate measurement of the wall shear stress, exerted by the flow of blood or a blood analog fluid requires a new measurement technique. This new method, presented in chapter 4, involves the measurement of the response of a sensing element, attached to the wall of the model, to the wall shear stress. A highly deformable gel layer will be used as the sensing element. The wall shear stress, exerted by the fluid, deforms the gel layer slightly. The small deformation of the gel layer can be measured accurately by means of speckle pattern interferometry (SPI). Through the properties of the gel layer, the wall shear stress can be inferred from the measured displacement. The preliminary results, flow depended wall shear stress measurements with a Newtonian fluid under steady flow conditions in a rectangular duct, are promising.
The report is concluded with a discussion and recommendations for future research.

Chapter 2

Blood: morphology and rheology

2.1 Introduction

Blood is a complex fluid consisting of the blood cells suspended in plasma. An outline of the composition of suspended blood cells is given in table 2.1.

cells	number per mm^3	unstressed shape and dimension μm	volume concentration in blood %
erythrocytes	$4 - 6 * 10^6$	biconcave disc 8x1-3	45
leucocytes	$4 - 11 * 10^3$	roughly spherical 7-22	1
platelets	$2.5 - 5 * 10^5$	rounded or oval 2-4	

Table 2.1: *blood cells [from Caro* et al. *(1978)]*

Further discussion of the blood cells will be confined to the red blood cells and the platelets. The red blood cells, or erythrocytes, occupy 45 % of the blood volume and dominate the rheological behavior of blood. The platelets are much less numerous and smaller but are included in this study because it is believed that they are involved in the development of atheroma (Caro *et al.* (1978)).

2.2 Morphology and properties of the main constituents of blood

This review on the composition and properties of the constituents of blood is limited to plasma, being the suspending phase, and red blood cells and platelets. The information for this section is taken from Caro *et al.* (1978), Merrill (1969), Chien (1979), Burton (1965) and Cokelet (1972).

2.2.1 Plasma

Plasma is the continuous liquid medium in which the blood cells are suspended. It is an aqueous saline solution with proteins. The outline of the composition of the plasma is given in table 2.2. The density of plasma is $1.03 * 10^3\ kg/dm^3$. If denaturisation of the proteins is avoided, plasma behaves like a Newtonian fluid with a dynamic viscosity of $\eta = 1.2\ mPa.s$.

material	concentration $g/100ml$	molecular weight $*10^{-3}$	molecular dimension nm
water	90-92		
proteins			
albumin	3.3-4.0	69	15x4
$\alpha_1$globulins	0.31-0.32	44-200	
$\alpha_2$globulins	0.48-0.52	150-300	
βglobulins	0.78-0.81	90-1300	20-50
γglobulins	0.31-0.32	160-320	23x4
fibrinogen	0.34-0.43	400	50-60x3-8
inorganic constituents			
cations			
sodium	0.31-0.34		
potassium	0.016-0.021		
calcium	0.009-0.011		
magnesium	0.002-0.003		
ations			
chloride	0.36-0.39		
bicarbonate	0.20-0.24		
phosphate	0.003-0.004		

Table 2.2: *Composition of plasma [from Caro* et al. *(1978)]*

The inorganic constituents of the plasma are a governing factor in various transport processes and generate an osmotic pressure of about $8 * 10^5\ Pa$ (equivalent to a 0.9% sodium chlorine solution by weight).
The proteins have various functions and can be divided into three groups:

- fibrinogen: a large, asymmetric molecule that is intimately concerned with the coagulation of blood. Although the concentration of fibrinogen is low, it attributes significantly to the elevated viscosity of plasma due to its asymmetry.
- albumin: a small molecule that is important for the osmotic pressure of the proteins.
- globulins: a relatively symmetric molecule that is involved in transport of lipids and antibody reactions.

Apart from the buffering function of all the proteins, both fibrinogen and the globulins are involved in the aggregation of the erythrocytes.

2.2.2 Erythrocytes

The erythrocytes form the dominant particulate matter of blood. The volume concentration of the erythrocytes, called haematocrite (HT), is about 45 %. The density of the erythrocytes is

$1.08 * 10^3\ kg/m^3$. The erythrocyte is a biconcave discoid and the main dimensions are given in figure 2.1. The origin of the biconcave shape of the erythrocyte is a source of dispute. For a review of possible explanations, one is referred to Fung (1993). An important consequence of the biconcave shape is the ability of the erythrocyte to change shape without changing the surface area.

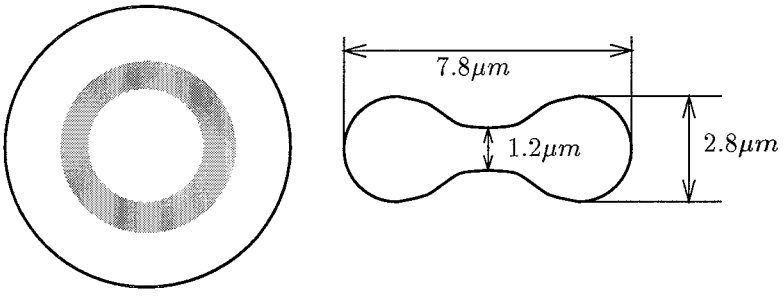

Figure 2.1: *Size and dimension of the erythrocyte*

The membrane of the erythrocyte has a thickness of 80 nm and consists of a phospholipid bilayer. This bilayer is covered with albumin at the outside and with another layer of protein, spectrin, at the inside. The spectrin layer is a skeletal protein and supports the lipid bilayer (figure 2.2).

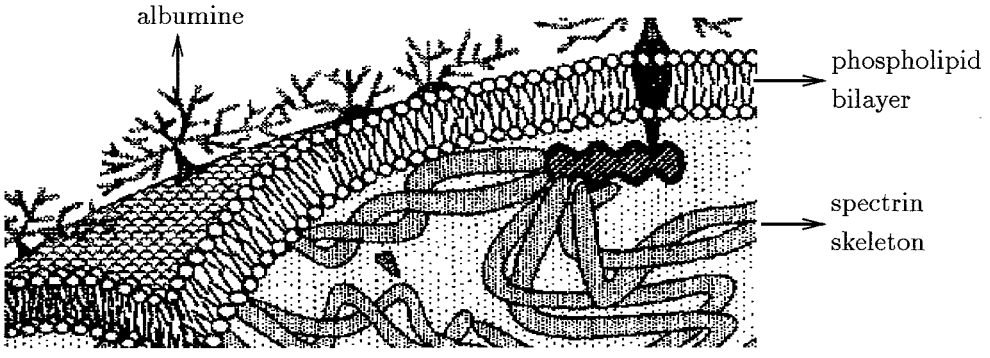

Figure 2.2: *Membrane of the erythrocyte [from Burton (1965)]*

The liquid interior of the erythrocyte is a saturated solution of haemoglobin (32 % by weight), behaving as a Newtonian fluid with a dynamic viscosity of $\eta = 6\ mPa.s$.
The haemoglobin ($MW = 68.000$) is a protein complex, consisting of an Fe^{2+} complex, the haem group, surrounded by aminoacid molecules. The haem group is essential for transport processes for it can bind oxygen and carbondioxide and gives blood its red color.
The biconcave shape, combined with the low bending stiffness of the membrane and the liquid interior, enhance the ability of the erythrocyte to deform readily. This enables the erythrocyte to pass through capillaries with a diameter smaller than 8 μm. Another phenomenon, closely linked to the deformability of the erythrocyte, is the rotation of the membrane around the liquid interior in a shear flow (tank-threading movement, Schmid-Schönbein *et al.* (1971)).

The erythrocytes aggregate face to face if they are brought in contact with each other at low shear rates (figure 2.3).

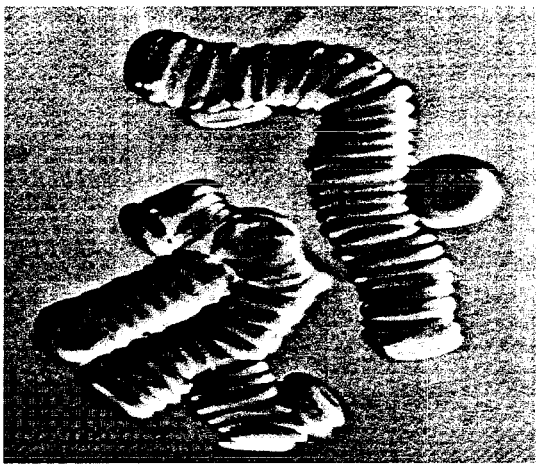

Figure 2.3: *Rouleaux of erythrocytes [from Burton (1965)]*

These aggregates are known as rouleaux and are formed under the influence of bridging macromolecules, especially fibrinogen. At near zero shear rates, secondary aggregation of the rouleaux occurs, leading to formation of a rouleaux network.

2.2.3 Platelets

The volume concentration of the platelets is 0.3 % and there is one platelet for every 10 erythrocyte. The platelets are small oval bodies with a phospholipid membrane and an interior that resembles the interior of regular cells. This includes a cytoskeleton, giving the platelet a much higher rigidity than the erythrocyte. If the platelets are brought in contact with adenosine diphosphate (ADP) they aggregate and a thrombus can be formed. The process of thrombus formation is very complex and various agents are involved.

2.3 Rheology of blood

The composition of blood, as well as the properties of its constituents, lead to a complex rheological behavior of blood. The research on the flow behavior of blood can be divided into two classes: one involved with the viscometric flow of blood and another dealing with blood flow in tubes. The viscometric studies are mainly focused on obtaining constitutive equations for blood. Generally, these constitutive equations can be used to relate stresses to deformation rates, and can be used to compute wall shear stresses from measured wall shear rates. In viscometry however, homogeneity the fluid and a constant shear rate are assumed and from several studies it can be concluded that this assumption does not hold for blood or concentrated suspensions in general (e.g. Karnis *et al.* (1966), Philips *et al.* (1992)). The review on the studies of blood and blood analog fluids in tube flow shows that the concentration distribution is inhomogeneous and that the velocity distribution is governed by the non-Newtonian properties of blood. Only if the shear rates and the concentration distributions in the viscometric devices can be measured and if the results are comparable to the physiologically relevant tube flow, the viscometric results can be used to relate measured wall shear rates to the wall shear stress.

2.3.1 Simple shear flow

Viscosity measurements of blood

The deformability, orientation and the aggregation of the erythrocytes induce the complex behavior of blood in simple shear flow, the prevailing flow condition at near-wall sites in the vascular tree. At low shear rates ($\dot{\gamma} =< 10\ s^{-1}$), the erythrocytes tend to aggregate and form rouleaux. The time scale for the formation of rouleaux is 10[s] (McMillan *et al.* (1987)). These rouleaux increase the viscosity of the blood. Decreasing the shear rate even further ($\dot{\gamma} =< 1\ s^{-1}$), the rouleaux form three dimensional structures, inducing an additional increase of the viscosity. If the shear rate is increased, the rouleaux break up and the erythrocytes align with the flow. Eventually, the shear rates are high enough deform the erythrocytes, thus decreasing the viscosity. The deformability, orientation and aggregation of the erythrocytes result in shear thinning behavior of blood in simple shear (figure 2.4).

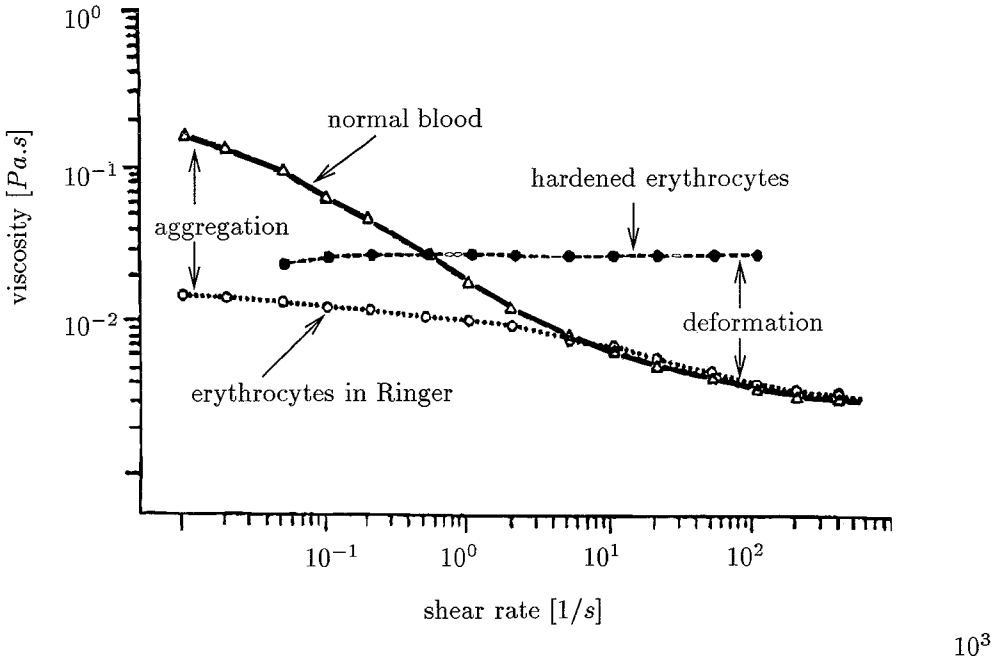

Figure 2.4: *Viscosity in steady shear of normal blood, blood with hardened erythrocytes (no deformation) and blood in a Ringer solution (no aggregation) [from Chien* et al. *(1969)]*

The deformability and the orientation of the rouleaux and the individual erythrocytes lead to the viscoelastic behavior of blood. They provide a mean of storing energy during flow. Thurston (1973) investigated the viscoelastic properties of blood in the linear viscoelastic regime and measured a significant elastic component in oscillatory blood flow (figure 2.5).

McMillan *et al.* (1987) investigated the transient properties of blood in viscometric flow. They measured the shear stress generated by blood, subjected to a number of sequential steps in the shear rate (figure 2.6). The overshoot in the shear stress was attributed to orientation of erythrocytes. The delayed relaxation of the shear stress can be related to the viscoelastic properties of blood and a rapid loss of orientation of the erythrocytes. The erythrocytes oriented after a total strain (shear rate multiplied by time) of 10.

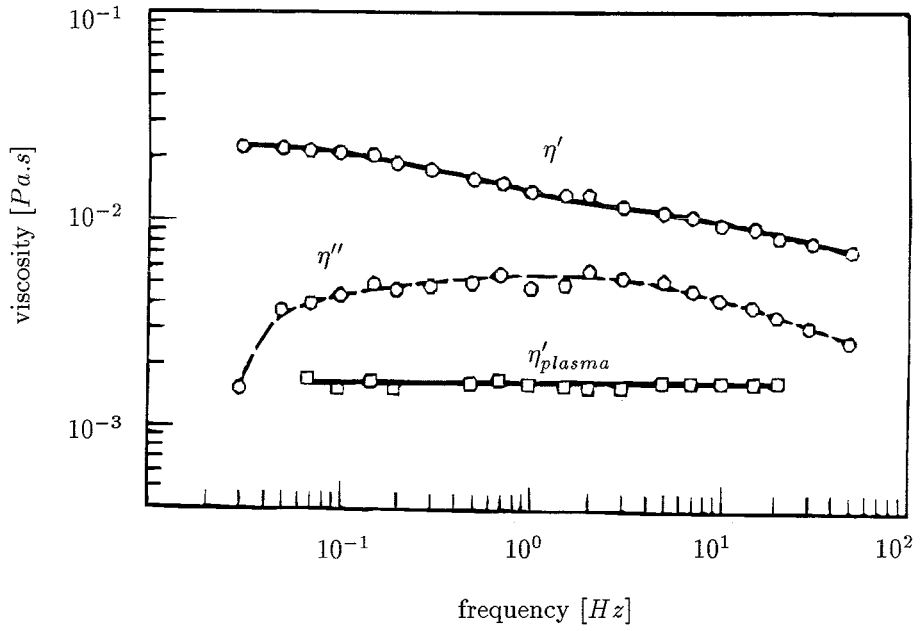

Figure 2.5: *The elastic (η'') and the viscous (η') component of the complex viscosity of blood as a function of frequency in oscillatory shear [from Thurston (1973)]*

Concentration and velocity measurements

Cokelet (1972) presented an extended review on the problems arising in determining the properties of blood through viscometry. The measured torque at low shear rates is a function of time, indicating migration of erythrocites and subsequent formation of a plasma rich layer near the wall. Reduction of the measured torque and rotational speed of the viscometer to shear stress and shear rate is not valid due to inhomogeneity of the fluid. Several studies confirmed these results. Karnis *et al.* (1966) measured velocity and concentration distributions in concentrated suspensions in a Couette device. They showed that the concentration distribution was not uniform and the velocity gradient was not constant. Philips *et al.* (1992) showed that the assumption of homogeneity of the concentration and velocity distribution in a Couette device with a relatively large gap is disputable for concentrated suspensions in general. A detailed analysis of the velocity and concentration distribution of the particles in the suspension in viscometric flow is necessary to be able to compare the measured wall shear stress to the velocity and concentration distribution in a physiologically relevant flow.

2.3.2 Tube flow

The importance of detailed analysis of flow behavior of blood at near-wall sites for the determination of wall shear stresses was pointed out in the previous section. A small selection of the available *in-vivo* experiments is given to indicate the existence of inhomogeneous erythrocyte and platelet concentration distribution and to show that the non-Newtonian properties of blood have a significant influence on the velocity distribution. Since the high concentration of blood cells is believed to have a major influence on the flow behavior of blood, reports on *in-vitro* experiments on diluted suspensions of blood cells are discussed only briefly. Although the vast majority of the experimental data are limited to flow in arterioles or very small tubes, their importance for the study of the near wall flow behavior is evident because in both cases the

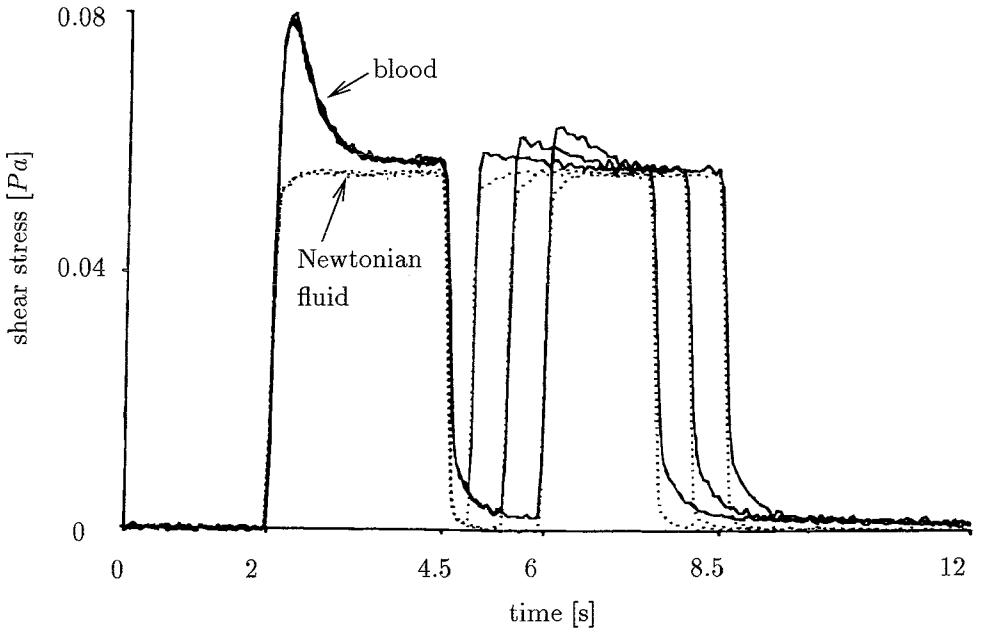

Figure 2.6: *Transient behavior of blood: measured shear stress after repeated steps in shear rate [from McMillan* et al. *(1987)]*

particulate nature of blood can not be ignored.

in-vivo Experiments

The inhomogeneity of the erythrocyte concentration distribution in small and medium sized arteries is well established. A cell-free layer exists near the vessel wall due to a physical exclusion effect. Despite its small dimension, the cell-free plasma layer is believed to have a profound effect on the flow of blood (Karnis *et al.* (1966). The existence of this cell-free layer was found *in-vivo* by Phibbs (1968). By quick-freezing an artery of a rabbit, the blood solidified and the concentration distribution and orientation of erythrocytes was determined. They found a very thin layer of low concentration immediately next to the vessel wall under steady flow conditions. The erythrocytes showed an orientation in the direction of the flow, especially in the center of the vessel. The preference of the erythrocytes to orientate in the flow direction increased significantly under pulsatile flow conditions.

Tangelder *et al.* (1986) studied velocity distributions in arterioles. By labeling the platelets and the erythrocytes with a fluorescent dye and applying microscope techniques, they were able to measure velocity distributions in the arterioles and the venules during the systolic and the diastolic phase. Using the small platelets as natural markers of the flow, they were able to determine velocities as close as 0.5 μm from the wall. The velocities of the platelets and the erythrocytes were comparable and the profiles, in both the arterioles and the venules, were flattened as compared to parabolic profiles (figure 2.7). They showed the presence of steep velocity gradients at near wall sites. Furthermore, they conclude that all the blood cells can come in contact with the vessel wall.

Woldhuis (1993) studied platelet distribution in arterioles and venules, using the same technique as Tangelder *et al.* (1986). A marked difference could be observed: in the arterioles

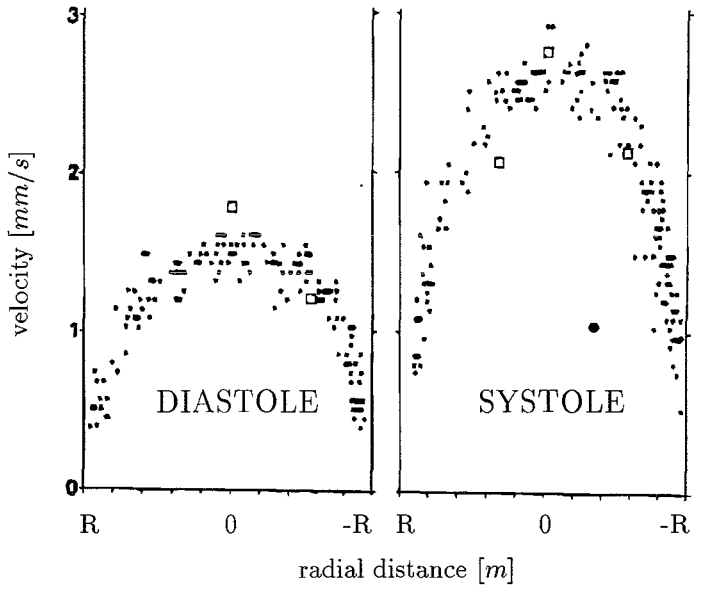

Figure 2.7: *Velocity distribution in an arteriole at diastole and systole ($D = 25\ \mu m$) [from Tangelder* et al. *(1986)]*

platelet concentration was relatively high near the wall and low in the center of the vessel while the distribution in the venules shows the opposite features (figure 2.8). The effect is attributed to erythrocytes behavior and/or geometry effects.

in-vitro experiments

The behavior of isolated particles in tube flow has been investigated extensively. The main object of these studies was that from understanding the behavior of an isolated particle a good model for the flow of concentrated suspension could be deducted. Rotation of particles in Poiseuille flow, axial migration of deformable particles, deformation under shear etc. were studied. From studies in concentrated suspension it is obvious that the models for particle flow, originating from studies in diluted suspensions, bear little or no resemblance to the behavior of particles in concentrated suspensions. Recent reviews of the research in *in-vitro* experiments on blood flow are given by Goldsmith (1993) and Wang and Hwang (1992).

Goldsmith and Marlow (1979) investigated the flow of a concentrated suspension of transparent ghost cells in small tubes ($32\ \mu m < R < 80\ \mu m$) under stationary flow conditions. They used erythrocytes, hardened erythrocytes and latex spheres as tracer particles and studied velocity and concentration distributions as well as particles paths of the tracers. The axial velocity, being the same for all tracer particles, showed a blunted profile (figure 2.9). The blunting of the velocity distribution increased with decreasing flow rate and increasing concentration of ghost cells. The degree of blunting also decreased with increasing diameter of the tube. The wall shear rates were sensitive to the blunting of the velocity profile: compared to a parabolic velocity distribution, up to three times higher wall shear rates were observed.
The rotation of tracer particles was observed but could not be matched with the theoretical predictions for rotation of particles in diluted suspensions. The tracers spend a considerable amount of time aligned with the axis of the tube. Rotation of the membrane of the erythrocyte tracers

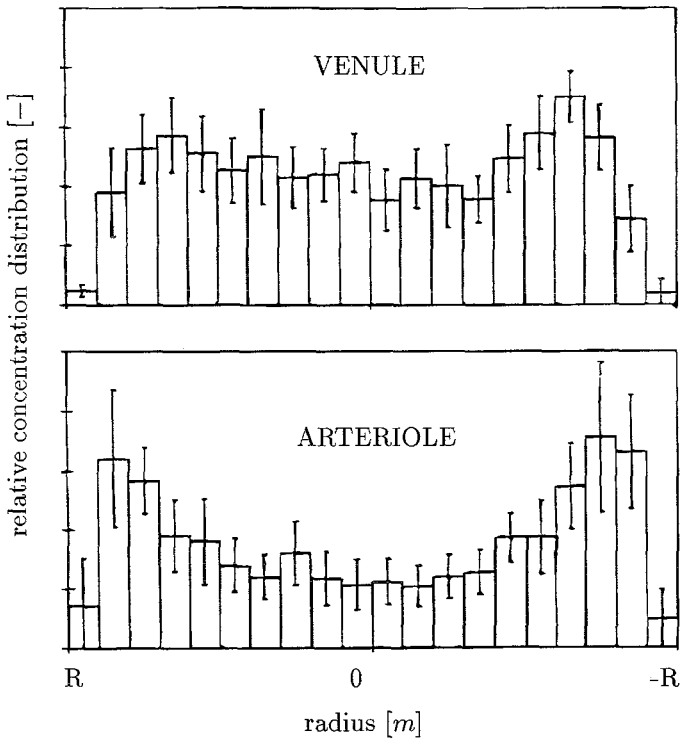

Figure 2.8: *Concentration distribution in arteriole and venule [from Woldhuis (1993)]*

was observed. The particle paths showed that the tracers exhibited erratical displacement in radial direction. The radial displacement was large in the area $0.4 < R < 0.8$, being smaller near the tube axis and the tube wall. The particle paths near the wall show that the tracers frequently collide with the wall. In the core of the tube, relatively large radial displacements of the tracer particles were found despite the uniform axial velocity. From the observed particle paths, an estimate for the dispersion coefficiënt was obtained. The concentration distribution showed a surprising result: at physiological concentration of the ghost cells, the erythrocyte tracers redistributed at higher flow rates from an almost uniform distribution at the entrance to a distribution with a significant shift of concentration towards the periphery further downstream (figure 2.10). This redistribution was strongly depended on the concentration and flow rate.

Cokelet and Goldsmith (1991) extended the study of Goldsmith and Marlow (1979) by measuring the hydrodymamic resistance, a measure for the wall shear stress, at very low flow rates. They observed an increase of the hydrodynamic resistance at decreasing mean tube velocity due to the formation of rouleaux. At even lower flow rates, the rouleaux showed inward migration and formed a compact network, decreasing the hydrodynamic resistance. The size of the peripheral cell depleted layer decreased with increasing concentration and increasing radius.

Bugliarello and Sevilla (1970) studied steady and pulsatile human blood flow in 40 and 70 μm glass tubes. They conclude that the plasma layer thickness under steady flow conditions depends on the HT only, decreasing in size with increasing HT. The pulsatile velocity profiles were in phase with the pressure gradient, indicating no significant influence of inertia. The thickness of the peripheral cell-depleted layer was not influenced by the pulsatility of the flow.

The influence of the flow rate and the concentration of the erythrocytes on the diffusion of

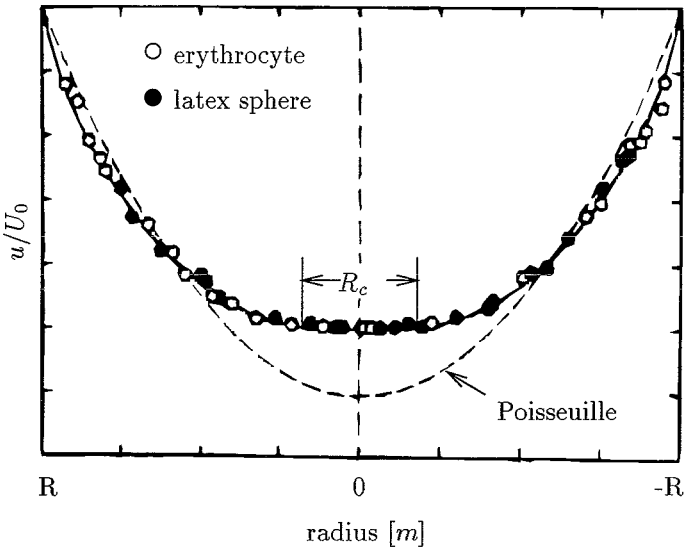

Figure 2.9: *Velocity distribution of various tracer particles in a concentrated ghost cell suspension in a small tube ($D = 39\ \mu m$) [from Goldsmith and Marlow (1979)]*

platelets was studied by Aarts *et al.* (1986). They measured platelet adhesion to the tube wall to evaluate the diffusivity of the platelets under steady flow conditions. The diffusivity increased with increasing concentration of the erythrocytes and with increasing wall shear rate, indicating enhanced radial migration of the platelets.

Karino and Goldsmith (1979) studied particle aggregation in whole blood in an annular vortex behind a tubular expansion. Both erythrocytes and platelets aggregated in the vortex, due to an increased collision frequency. The aggregates moved towards the center of the vortex and remained trapped. Platelets also adhered to the tube wall, indicating an increased platelet collision with the wall due to the presence of the erythrocytes. It was also shown that after coating the glass tube with collagen, a concentration of platelet adhesion could be seen in the surroundings of the reattachment point.
From the above cited literature, it is obvious that the non-Newtonian properties of blood significantly alter the velocity distributions, and therefore the shear rates, in small tubes. The predilection of the atherosclerotic lesions for the larger and medium sized arteries necessitates a research on the influence of the non-Newtonian properties of blood on the flow in those arteries. The carotid artery bifurcation serves as a model and the steady flow patterns, using a blood analog fluid, are presented in chapter 3. Since the results of viscometric studies can not be transposed to physiologically relevant flow conditions directly, the estimation of near wall viscosity poses major difficulties. This instigated a research for a new method to measure the wall shear stress and this method will be discussed in chapter 4.

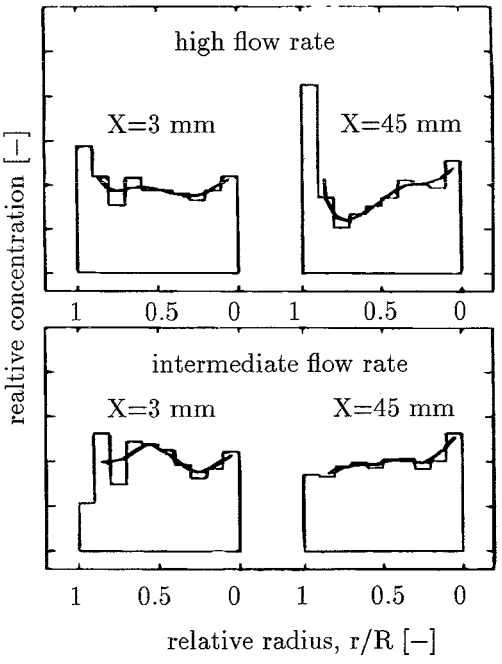

Figure 2.10: *Concentration distribution of erythrocytes in a concentrated ghost cell suspension in a small tube ($D = 39\ \mu m$) [from Goldsmith and Marlow (1979)]*

Chapter 3

Viscoelastic flow in a three dimensional model of the carotid bifurcation: LDA experiments

3.1 Introduction

Local haemodynamics are believed to play an important role in the development of those lesions. The predilection of atherosclerosis for the sinus of the carotid bifurcation (figure 3.1) is believed to be related to low or oscillating shear rates or shear stresses (Caro *et al.* (1971), Nerem (1992)).

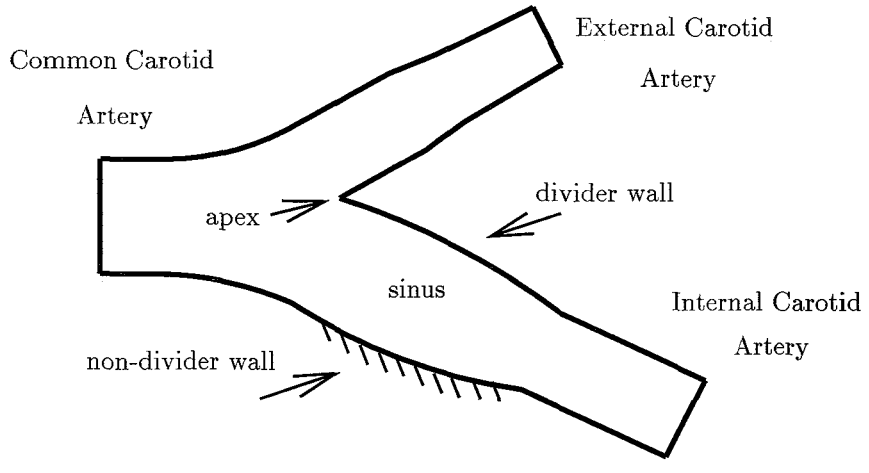

Figure 3.1: *Schematical representation of the carotid bifurcation*

The local haemodynamics are not only governed by the pressure pulse and the geometry of the bifurcation but also by the fluid properties. Blood can be envisioned as a concentrated suspension of flexible, asymmetric particles (erythrocytes) in Newtonian liquid (plasma), exhibiting shear thinning and viscoelasticity. In this chapter, the study on the influence of the non-Newtonian properties of a blood-analog fluid on the flow field in a rigid model of the carotid bifurcation under stationary flow conditions will be described.
Several studies dealt with stationary flow patterns in three dimensional models of the carotid bifurcation, using a Newtonian fluid. Bharadvaj *et al.* (1982) found a complex flow field in the internal carotid artery in which secondary flows played an important role. They localized

a region with low velocities near the non-divider wall that extended with increasing Reynolds number. At the divider wall of the carotid sinus a high shear region with high axial velocities was found, separated from the low shear region by a shear layer. The experiments and computations in steady flow of Rindt *et al.* (1990) confirmed these results.
A number of numerical studies employed generalized Newtonian fluid behavior to compute the flow field in the carotid bifurcation. In these studies, only the shear thinning behavior of blood is taken into account. Perktold *et al.* (1991) used the Casson model to compute instationary flow in a three dimensional model of the carotid bifurcation. They observed slightly flattened velocity profiles in the common carotid artery. In the carotid sinus, the secondary velocities were somewhat lower and the region of flow reversal slightly smaller for the non-Newtonian fluid. Despite these small differences, no significant influence of the shear thinning on the large scale flow phenomena in the internal carotid artery was found. These results compare well to the study of Baaijens *et al.* (1993), who investigated the effect of a power law and a Casson fluid on steady flow field in a two dimensional model of the carotid bifurcation. They also found a flattened axial velocity distribution and lower secondary velocities for the generalized Newtonian models. Ballyk *et al.* (1994) focused their numerical study in an end-to-side anastomosis on the effects of non-Newtonian fluid properties on the wall shear stress distribution. They applied a generalized power law fluid and, compared to the Newtonian fluid, found small differences in the amplitude of the wall shear stress under steady flow conditions. The differences in the magnitude of the wall shear stress disappeared under pulsatile flow conditions. None of the above studies incorporated the viscoelastic behavior of blood because the available codes could not handle three dimensional viscoelastic flow problems.
Experimental studies on viscoelastic flow in larger arteries are relatively sparse but indicate a significant influence of the viscoelasticity of the fluids on the flow phenomena. Liepsch and Moravec (1984) investigated the flow in a rigid 90° bifurcation under steady flow conditions. They found a striking influence of the non-Newtonian properties of a polyacrylamide solution on the axial velocity distribution. Especially the size and the location of the region of flow reversal were affected by the viscoelasticity. Ku and Liepsch (1986) studied the axial velocity distribution in a 90° bifurcation under pulsatile flow conditions, also using a polyacrylamide solution. They found a reduction of the size of the region with flow reversal for the non-Newtonian fluid in a rigid model. In an elastic model, the size and the location of the region with flow reversal changed significantly under the influence of the viscoelasticity of the fluid. Mann and Tarbell (1990) applied a flush mounted hot film anemometer to evaluate the influence of non-Newtonian fluids on the magnitude of the wall shear rates. They compared the shear rates of one Newtonian and three blood analog fluids in a bend and found significantly higher wall shear rates in oscillatory flow for the viscoelastic fluids, especially at the inner curvature.
A detailed analysis of the axial and secondary velocity distribution in a model of the carotid bifurcation using a viscoelastic fluid enables a direct comparison with the numerical results and the importance of the viscoelasticity of blood can be evaluated. In this chapter, a blood analog fluid will be presented that can be used for LDA measurements in a Plexiglass model of the carotid bifurcation. Both axial and secondary velocities will be presented and it will be shown that the viscoelastic properties of the blood analog fluid significantly influence the flow patterns in the carotid bifurcation. The wall shear rates at the divider wall and the non-divider wall will be compared.

3.2 Experimental methods

3.2.1 Model of the bifurcation

The geometry of the three dimensional model of the carotid bifurcation (figure 3.1) was derived from Bharadvaj *et al.* (1982). The 1:1 model was machined out of PMMA (Plexiglass) with a refraction index of 1.491, and was identical to one used in the study of Rindt *et al.* (1990).

3.2.2 Blood analog fluid

The shear thinning and viscoelasticity of blood are closely related to its microscopic structure. The red blood cells determine the rheological behavior of blood: both shear thinning and viscoelasticity are related to aggregation, deformation and alignment of the red blood cells. A suitable blood analog fluid should include these non-Newtonian properties. Application of the fluid for LDA measurements in a three dimensional Plexiglass model imposes two additional requirements on the blood analog fluid: transparency and a matched refraction index. A concentrated solution of potassium thiocyanate (KSCN, 71 % by weight) meets the latter two demands and addition of 200 *ppm* Xanthan-gum (95465 Fluka) results in shear thinning and viscoelastic behavior. Viscometric experiments, using a cone-plate viscometer (RFSII, Rheometrics), showed that an excellent agreement was obtained for the shear thinning behavior but that the elastic component of the KSCN-Xanthan gum solution (KSCN-X) was too high (figure 3.2).

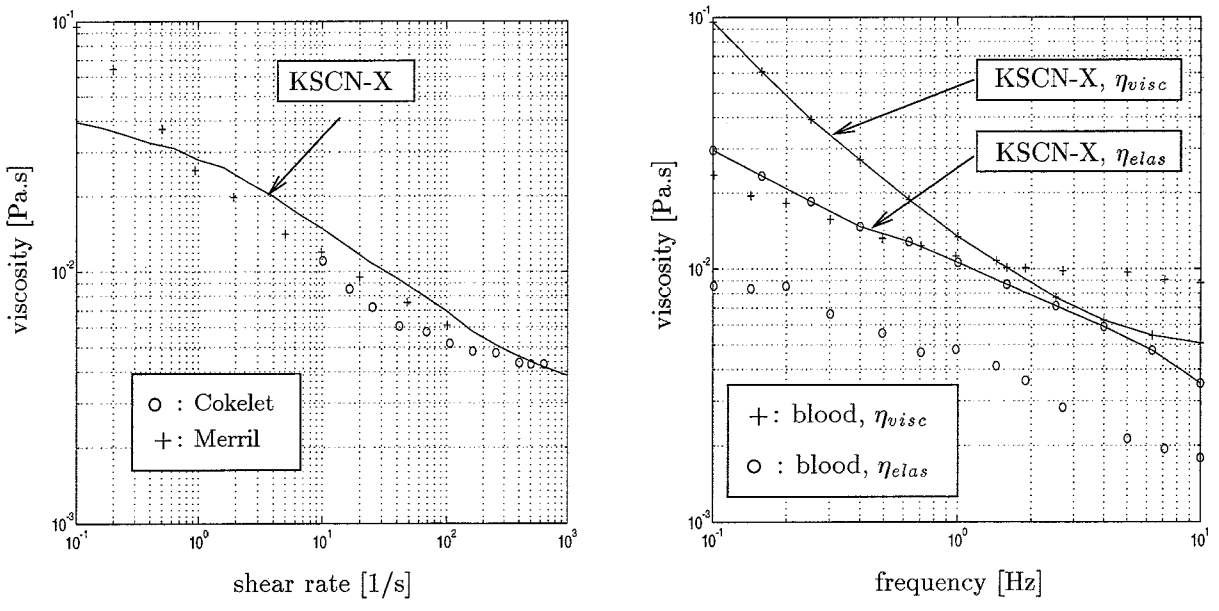

Figure 3.2: *Steady shear viscosity of KSCN-X (left) compared to the blood measurements of Merrill (1969) and Cokelet (1972) and linear viscoelasticity of KSCN-X (right) compared to the results of Thurston (1973) of blood measurements in oscillatory flow.*

The microscopic mechanism responsible for the viscoelastic properties of the analog fluid will generally differ from those described for blood, and thus it is not likely that a complete match of all rheological properties of blood can be found, using fluids that are governed by other

microscopic mechanisms. The excellent match of the shear thinning behavior enables a detailed study of the relative importance of the viscoelastic behavior on flow phenomena in the carotid bifurcation by comparing the experimental results to the numerical simulations of Perktold *et al.* (1991).

3.2.3 Fluid circuit and LDA apparatus

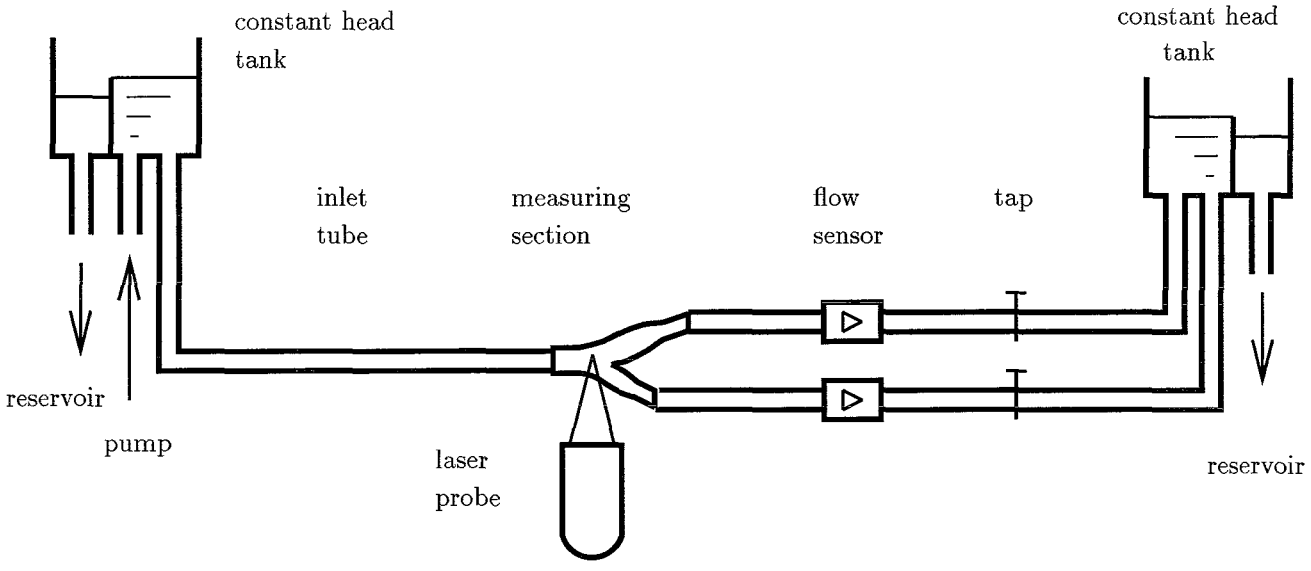

Figure 3.3: *Schematic presentation of the fluid circuit.*

A schematic presentation of the fluid circuit is given in figure 3.3. The reservoir containing the measuring fluid was immersed in a container filled with water that was kept at a constant temperature ($36°C$). A roller pump (N-4504, Drake-Willock) was used to pump the fluid to a constant head tank. This constant head tank was successfully employed to eliminate cyclic disturbances of the stationary flow caused by the roller pump. Before entering the model of the carotid bifurcation, the fluid passed through an inlet tube of length 150 D where D represents the diameter of the common carotid artery. This inlet tube was necessary to guarantee a stable and fully developed flow as the KSCN-X enters the measuring section. Return tubes with tabs and flow sensors (Transflow 601, Skalar Instruments) transported the KSCN-X back to the reservoir. Titanoxide flakes (Iriodine 111, Merck) were added to the fluid in a concentration of about 20 $g \cdot m^{-3}$ to serve as seeding for the LDA measurements. The velocity measurements were performed by means of a two-component fiber optics LDA system in backscatter mode in combination with a Flow Velocity Analyser (58N20, Dantec). A 300 mW Argon-ion laser (5500A, Ion Laser Technology) generated a green ($\lambda = 514.5\ nm$) and a blue laser beam ($\lambda = 488.0\ nm$). Glass fibers transmitted the laser light to the measuring probe. A front lens with a focal length of 80 mm focused the laser beams to form a measuring volume ($50 \times 50 \times 200\ \mu m$).

3.2.4 Experimental procedure

The velocity measurements, using the Newtonian KSCN solution, were performed under stationary flow conditions. The dimensionless parameters describing the flow pulse, Re (Reynolds

number) and γ (flow division ratio), were defined as follows

$$Re = \frac{D \cdot U}{\nu}, \qquad \gamma = \frac{Q_E}{Q_C}, \tag{3.1}$$

where U represented the cross sectional mean velocity in the common carotid artery, D the diameter of common carotid artery, ν the kinematic viscosity of Newtonian KSCN solution and Q_E and Q_C the flow through the external and common carotid artery respectively. The experiments were performed for $Re = 270$ and $\gamma = 0.45$. Subsequently 200 ppm Xanthan gum was added to the KSCN solution and the measurements were repeated for identical flow and flow ratio. The velocity distribution was measured at one site in the common carotid artery and at three sites in the internal carotid artery (figure 3.4).

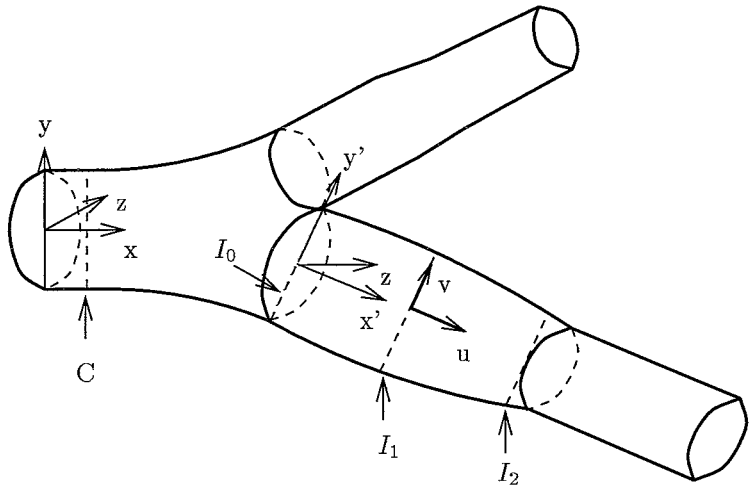

Figure 3.4: *Definition of measurement sites and velocity components*

The axial velocity in the common carotid artery was measured $3D$ upstream of the apex, along the y-axis. In the interna, both axial (u) and secondary (v) velocity distributions were mapped at I_0, I_1 and I_2, with a distance D between each site. The velocity signals were computed as the mean of 100 measurements. Only half of the planes in the internal carotid artery were mapped because of the expected symmetry. To check the validity of this assumption, I_0 for the Newtonian fluid and I_2 for the non-Newtonian fluid were measured completely.

3.3 Results

3.3.1 Velocity measurements

In figure 3.5 the axial velocity profile in the common carotid artery is given for the Newtonian and the non-Newtonian fluid. As the flow is fully developed, the axial velocity profile for the Newtonian fluid is parabolic. The velocity profile of the non-Newtonian fluid is flattened as expected for a shear thinning fluid.
In figures 3.6, 3.7 and 3.8 the axial (top) and secondary (bottom) velocity distribution for the Newtonian (left) and non-Newtonian (right) fluid in the internal carotid artery are presented in a three dimensional velocity plot combined with a contour plot. The results for the Newtonian fluid confirm the results of Rindt *et al.* (1990). Below these results will be compared with those obtained with the non-Newtonian fluid.

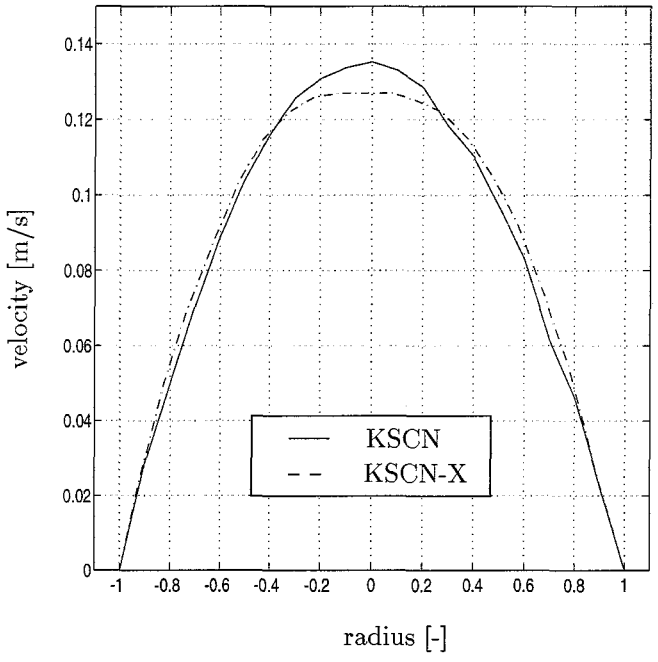

Figure 3.5: *Axial velocity distribution in the common carotid artery for the Newtonian fluid (KSCN) and the non-Newtonian fluid (KSCN-X)*

I_0: The axial velocity distribution for the Newtonian fluid shows that the assumption of symmetry is valid. The flow division at the apex results in high shear rates near the divider wall. For the KSCN-X solution, the velocity gradients are less steep. The axial velocity distribution shows significant flattening and higher velocities near the non-divider wall. The secondary velocities are predominantly directed towards the divider wall due to inertia of the fast moving fluid originating from the center of the common carotid artery. These secondary velocities are much lower for the non-Newtonian fluid.

I_1: The most prominent difference between the Newtonian flow and the viscoelastic fluid can be seen in the secondary velocity distribution. The secondary velocity, originating from the curvature induced Dean vortex, is remarkably lower. The consequences for the axial velocity distribution are obvious: the transport of particles with low velocity along the wall towards the center of the vessel is less dominant and the shift of the peak axial velocity towards the divider wall is nearly absent. The typical 'C'-shape in the contour plot of the axial velocity distribution, as present in the Newtonian case, can not be found. The axial velocity profiles are flatter and the peak axial velocity is significantly lower. The region of flow reversal, a combined effect of the Dean vortex and the divergence of the lumen, disappeared. The axial velocity near the non-divider wall remains positive.

I_2: The secondary velocities for the non-Newtonian fluid reveal the effect of the convergence of the lumen: the velocity at the divider wall and the non-divider wall are directed towards the center of the vessel. The Newtonian secondary velocity distribution is still dominated by the Dean vortex. As a consequence, a substantially lower axial velocity in the center of the vessel can be seen for the Newtonian fluid whereas the non-Newtonian fluid shows an almost fully recovered velocity profile.

3.3.2 Wall shear rates

The values for the axial wall shear rates at the divider wall and the non-divider wall were estimated using the axial velocity distribution in the symmetry plane. The near wall velocity distribution was extrapolated to the estimated position of the wall and the wall shear rates were computed. The values of the wall shear rates in table 3.1 must be considered as a rather crude approximation, since the method of computing the shear rates mentioned above is quite sensitive to the estimated position of the wall.

		Newtonian fluid	non-Newtonian fluid
I_0	D.W.	126	98
	N.D.W.	-4	4
I_1	D.W.	116	71
	N.D.W.	-3	6
I_2	D.W.	173	80
	N.D.W.	48	62

Table 3.1: *Estimated wall shear rates at the divider wall (D.W.) and the non-divider wall (N.D.W.)*

The wall shear rates at the divider wall are significantly lower for the non-Newtonian fluid (up to twice as high) whereas the shear rates at the non-divider wall are higher and positive at every site.

3.4 Conclusions and discussion

Laser Doppler anemometry was applied to obtain detailed quantitative information on the flow field in a three dimensional model of the carotid bifurcation for a Newtonian and non-Newtonian fluid. A concentrated KSCN solution with 200 *ppm* Xanthan gum, combining non-Newtonian properties with a high refraction index, served as a blood analog fluid. The small dimensions of the measuring volume enabled a detailed study of the flow phenomena in the bifurcation model. Several assumptions concerning the bifurcation model, the flow conditions and the blood analog fluid were made in this study. The model of the bifurcation was rigid and the compliance of the arterial tree downstream of the bifurcation was not taken into account. Ku and Liepsch (1986) found a significant influence of the distensibility of the wall, especially when using a viscoelastic fluid. The flow in the carotid artery is pulsatile and the unsteady flow features in models of the carotid bifurcation have been studied extensively (e.g. Ku and Giddens (1987) and Palmen (1994)). Although pulsatility influences the flow features during systole and the onset of diastole, steady flow conditions prevail at the end of diastole. The non-Newtonian properties of blood are well established (Thurston (1973)). The shear thinning of blood is matched excellently by the KSCN-X solution but the elastic component of the complex viscosity is too high. Direct comparison of the results of this study with velocity measurements in the carotid bifurcations from clinical practice is not possible because of the assumptions discussed above. By carefully controling the experimental conditions, this study provides detailed information of the relative influence of the viscoelasticity of the blood analog fluid on the flow patterns in the carotid bifurcation.
The velocity distribution for the Newtonian fluid in the internal carotid artery compares well to previous studies (Rindt *et al.* (1990), Bharadvaj *et al.* (1982)). The dominant features are

flow separation, secondary flow due to the curvature, flow reversal due to widening of the lumen and the effect of the convergence of the lumen. Differences between the measured flow fields of the Newtonian and non-Newtonian fluids in this study are evident. In the communis the non-Newtonian fluid shows a flattened axial velocity profile due to its shear-thinning behavior. In the interna, the non-Newtonian velocity field is flattened, has lower velocity gradients at the divider wall, and positive velocity gradients at the non-divider wall. The most obvious difference can be found in the secondary velocity distribution: the Dean vortex is much weaker and the secondary velocities are much lower. As a consequence, the axial velocity distribution is influenced significantly and the region with flow reversal disappears. The wall shear rates indicate that non-Newtonian fluid behavior decreases the magnitude of the shear rates at the divider wall whereas the values at the non-divider wall are significantly higher.

Perktold *et al.* (1991) investigated the flow in three dimensional bifurcation numerically, taking the shear thinning properties of blood into account only. The end-diastolic features of the flow field revealed only minor influence of the shear thinning on the axial velocity distribution. A comparison with the results from this study indicates a significant influence of the viscoelastic fluid behavior on the large scale flow phenomena in the carotid artery bifurcation. Furthermore, the near wall velocity distribution is influenced by the viscoelastic behavior of the fluid, as already indicated by Mann and Tarbell (1990). In studies, relating local haemodynamics to atherogenesis, the viscoelastic behavior of blood cannot be ignored.

The shear thinning and viscoelastic behavior of the fluid and a complex geometry of the carotid bifurcation all interact resulting in a complex flow field as described in this paper. This complexity prevents a detailed analysis of the attribution of shear thinning and viscoelasticity to the measured flow phenomena. Future experiments will be carried out in simpler geometries (e.g. 90° bend) to improve the understanding of the flow behavior of blood-analog fluids.

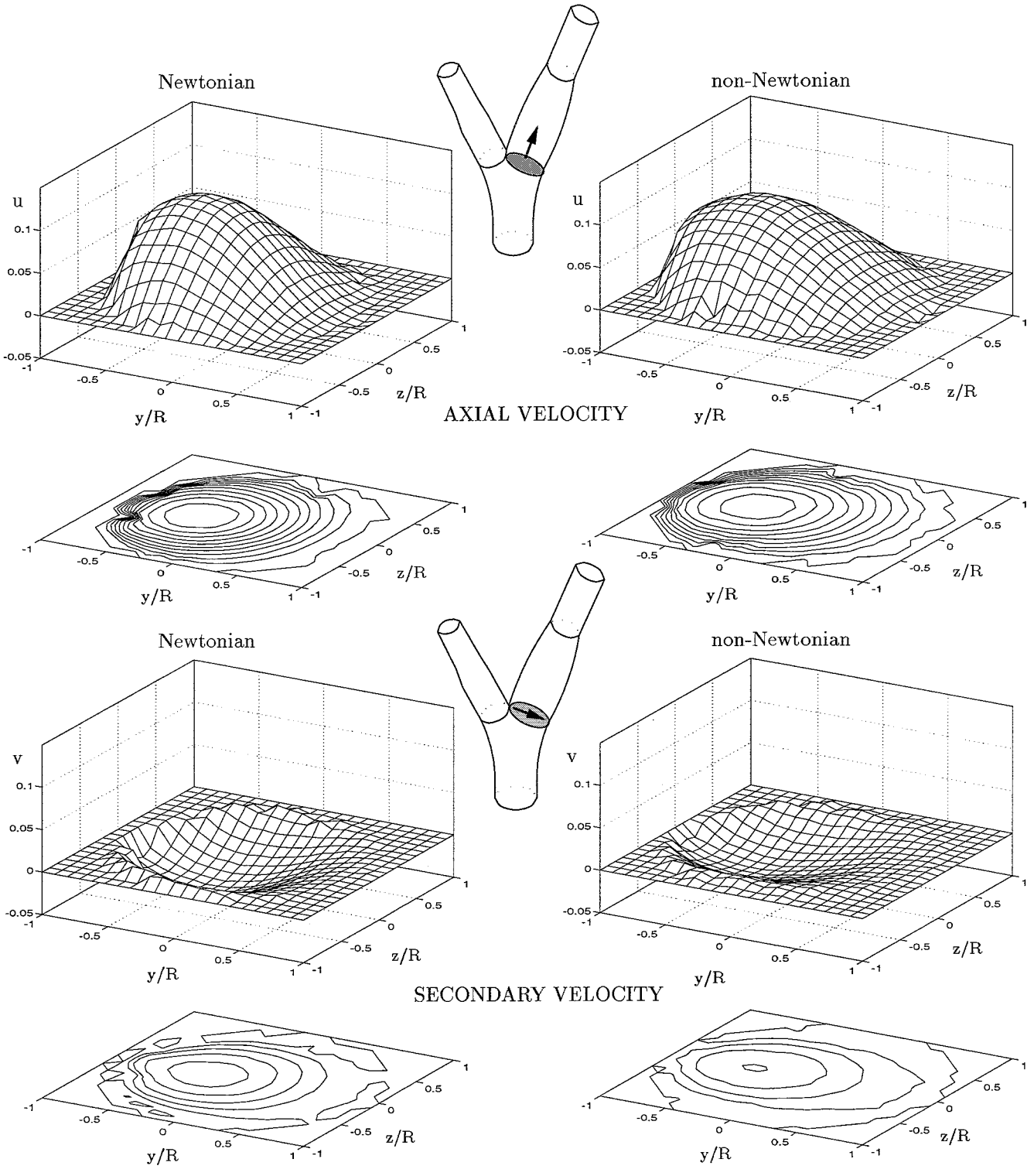

Figure 3.6: *Velocity distribution at site I_0*

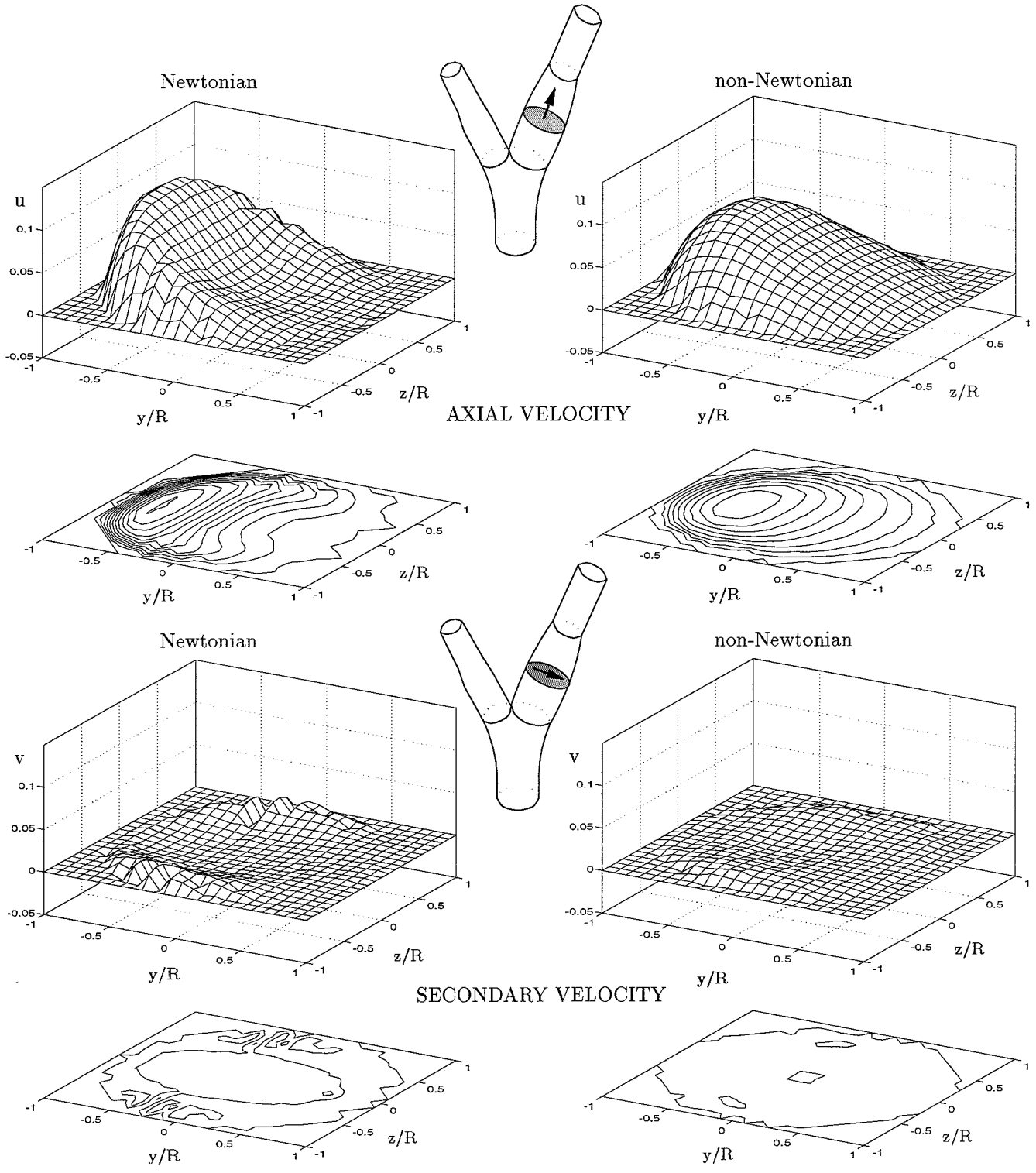

Figure 3.7: *Velocity distribution at site* I_1

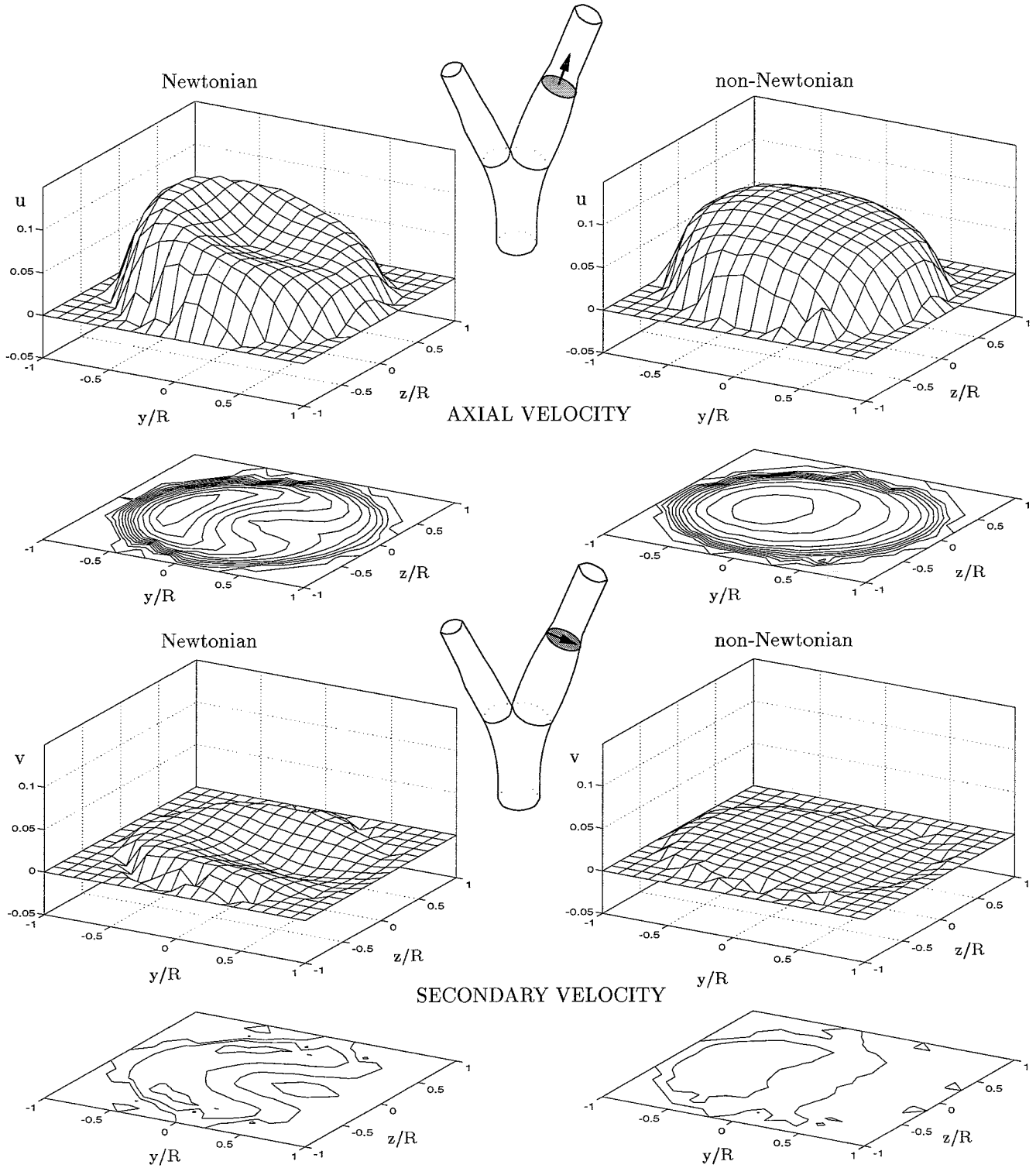

Figure 3.8: *Velocity distribution at site I_2*

Chapter 4

A new method to measure the wall shear stress

4.1 Introduction

The wall shear stress is defined as the product of the velocity gradient normal to the wall and the viscosity of the fluid at the wall. The wall shear stress values are usually determined by multiplying the wall shear rate, extrapolated from the measured velocity distribution, by the estimated viscosity. There are alternative methods to measure the wall shear rate: Mann and Tarbell (1990) applied flushed mounted hot film anemometry to compare the effect of the elasticity of several blood analog fluids on the wall shear rate distribution. A review on the available methods to measure the wall shear rate is given by Hanratty and Campbell (1983). The estimation of the viscosity of blood and blood analog fluids near the wall poses major difficulties. Blood is a concentrated suspension of blood cells in Newtonian plasma and its non-Newtonian properties are well established (Chien (1979)). The viscosity of the blood is governed by the suspended particles. Both in viscometric flow and in tube flow, the concentration distribution of the suspended particles in blood is not homogeneous (Goldsmith (1993), Karnis *et al.* (1966)). Therefor the viscosity of blood near the wall can not be inferred directly from viscometric experiments. An accurate measurement of the wall shear stress, exerted by the flow of a complex suspension as blood requires a different measurement technique.
Instead of focusing on the fluid, the response of a sensing element, attached to the wall, can be used to measure the wall shear stress. Tanner and Blows (1976) measured the thickness of an oil film in air flow and coupled the thickness variation to the wall shear stress distribution. Although the thickness of the oil layer was measured quite accurately, the method was inapt for measuring absolute values of the wall shear stress. Combined with its quasi-static nature, the application of this method in blood flow is limited. In aerodynamics, the wall shear stress in air flows is often measured using compact gauges that consist of a sensing element that can move parallel to the boundary of the wall. The deformation of the element, or the force required to keep it in its original position, is a measure for the wall shear stress. A review of the available gauges is given by Winter (1977). If the value of the wall shear stress is low, as expected in blood flow ($2 - 3$ Pa, Giddens *et al.* (1990)), an accurate measurement of the stress is only possible if the surface of the sensing element is relatively large, thus limiting the applicability of these devices in physiologically relevant geometries.
In this chapter, a new method to measure the wall shear stress will be presented (see also figure

4.1).

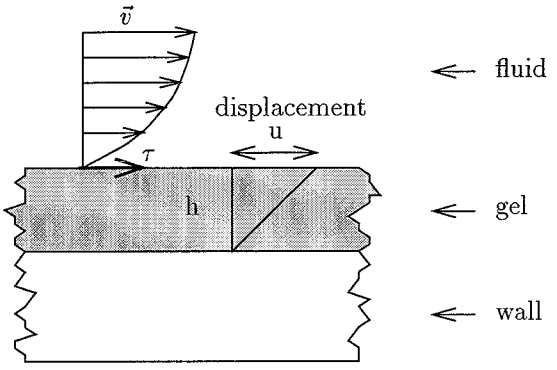

Figure 4.1: *Wall shear stress measurement through displacement measurement of a gel layer*

A highly deformable gel layer will be used as the sensing element. The gel layer is attached to the inner wall of a flow model. The wall shear stress, exerted by the fluid, deforms the gel layer slightly. The small deformation of the gel layer can be measured accurately by means of Speckle Pattern Interferometry (SPI). Through the properties of the gel, the wall shear stress can be inferred from the deformation of the gel layer using equation 4.1.

$$\tau = G \cdot (\frac{du}{dh}) \approx \frac{G}{h} \cdot u \tag{4.1}$$

where G is the bulk modulus, h the thickness and u the displacement of the gel layer. The aim of this research is to investigate whether the deformation measurement of a gel layer can be used to determine physiologically relevant wall shear stress values.

4.2 Experimental methods

The feasibility of the proposed method is assessed by measuring the wall shear stress in a rectangular duct. The deformation of the gel layer at the inner wall of the duct is measured by means of SPI. The principle of SPI will be explained briefly, followed by a description of the developed SPI apparatus and the flow cell. For further reading on SPI, one is referred to Jones and Wykes (1989) and Erf (1978).

4.2.1 SPI

When a monochromatic light source illuminates a diffusive surface, the reflected light interferes and a speckle pattern is generated. If two laser beams are used to illuminate the diffusive surface, the resulting speckle pattern can be used to measure small deformations or displacements of the surface (Jones and Wykes (1989)). The two laser beams each generate a speckle pattern, and the two speckle patterns interfere, resulting in an intensity distribution that can be recorded by e.g. a CCD camera.
This intensity distribution, also called irradiance, can be decomposed into the irradiances of the two separate speckle patterns and an interference term. It can be shown that the measured irradiance (I) can be written as:

$$I(\boldsymbol{x}, \delta) = I_1(\boldsymbol{x}) + I_2(\boldsymbol{x}) + 2\sqrt{I_1(\boldsymbol{x}) I_2(\boldsymbol{x})} cos(\theta(\boldsymbol{x}) + \delta) \tag{4.2}$$

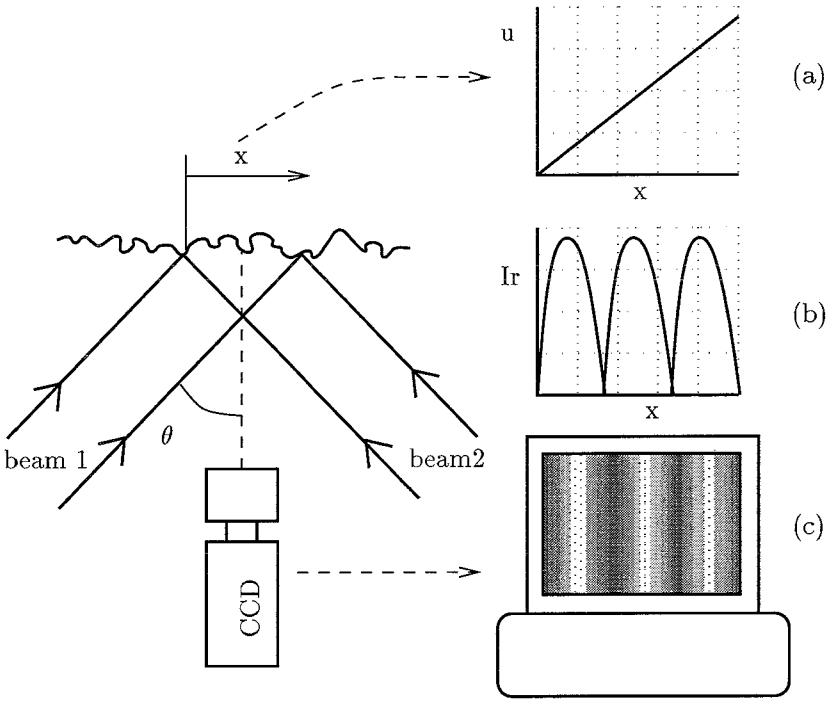

Figure 4.2: *In-plane displacement measurement with SPI: imposed displacement (a), expected irradiance distribution (b) and measured fringe pattern (c)*

where $\boldsymbol{x}$ denotes the position vector on the measured surface, $I_1(\boldsymbol{x})$ and $I_2(\boldsymbol{x})$ the irradiances of laser beam 1 and 2 respectively and the third term of the measured irradiance is the interference term. The contribution of the interference term to the measured irradiance depends on the phase difference (δ) between the two separate speckle patterns. If the surface is deformed, I_1 and I_2 remain unchanged while the phase difference between of the light waves reflected from the diffusive surface changes, and so will the contribution of the of the interference term in the measured irradiance. The phase difference δ depends on the displacement u of the surface and geometry of the speckle apparatus:

$$\delta = \frac{2 * sin(\theta) * 2 * \pi * \boldsymbol{u}}{\lambda} \tag{4.3}$$

where λ is the wavelength of the laser beam and θ the angle between the laser beam and the viewing direction of the CCD camera (see also figure 4.2). The relative phase will only change due to a displacement in the plane of the laser beams, perpendicular to the viewing direction. Only one component of displacement field of the surface can be monitored and the displacement measurements are not disturbed by out-of-plane movements. If the speckle pattern before deformation is recorded and subtracted from the resulting irradiance after deformation of the surface and averaged over an area with constant δ, the resulting intensity distribution (I_r) is:

$$I_r(\boldsymbol{x}, \delta) = 16\sqrt{I_1(\boldsymbol{x})I_2(\boldsymbol{x})} \mid sin\frac{\delta}{2} \mid \tag{4.4}$$

The measured irradiance distribution after video signal subtraction is a function of the phase difference δ and therefore also a function of the displacement u (equation 4.3).

In figure 4.2, a one dimensional surface is deformed, resulting in a linear displacement distribution (figure 4.2a). The argument of the sine function ($\frac{\delta}{2}$) in the irradiance after video subtraction also varies linearly with x and the expected irradiance distribution can be computed (figure 4.2b). Measurement of the speckle pattern before and after deformation and subsequent video subtraction by means of a computed controlled CCD camera yields the typical fringe pattern (figure 4.2c).

4.2.2 SPI apparatus

The developed SPI apparatus is schematically drawn in figure 4.3.

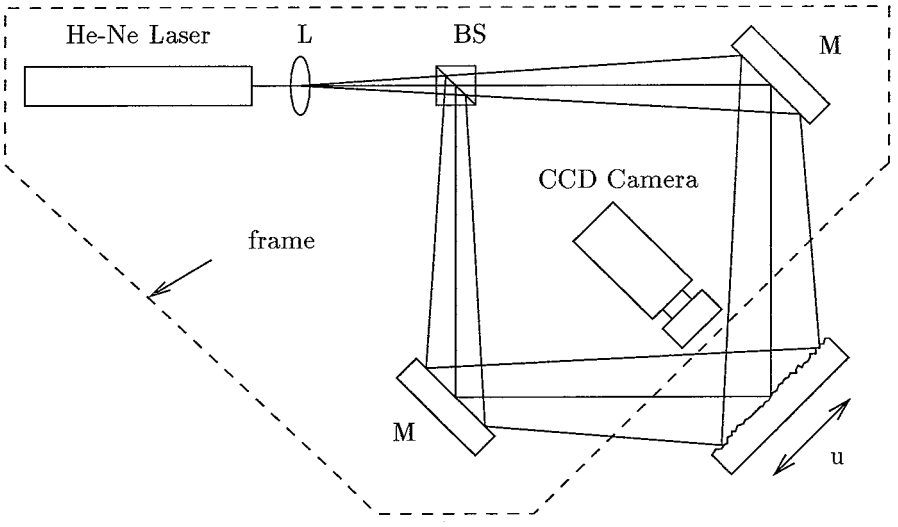

Figure 4.3: *SPI apparatus*

The 10 mW He-Ne laser (105-L, Spectra Physics) produces a laserbeam with a diameter of approximately 1 $[mm]$ and a wavelength of 632.8 $[nm]$. The laserbeam is expanded by the lens L and split by the beamsplitter BS. The two laserbeams, reflected by the adjustable mirrors M, eventually overlap on the surface of which the displacement u has to be measured. The $512x512$ pixels CCD camera (MXR, HCS) records the generated speckle patterns. The camera is connected to a PC with a frame grabber. An image processing package (TIM, Difa Measuring Systems) provides the necessary tools for the video signal subtraction. The position of individual components of the setup can be adjusted so the angle θ can be varied from 30° to 60° and the dimension of the investigated surface from $2x2$ mm^2 to approximately $40x40$ mm^2.

4.2.3 Experimental setup

The deformation of the gel layer in a rectangular duct was measured (figure 4.4), using water as a measuring fluid. Two constant head tanks provided a constant pressure gradient over the flow model, thus ensuring steady flow conditions in the setup. The flow model was a rectangular Plexiglass channel ($axbxL = 5*100*5000\,[mm]$) with the gel layer ($h_{gel} = 2.2\,[mm]$) attached to the lower wall. The flow rate through the duct was adjusted by controling the pressure gradient and was monitored by a flow meter (Transflow 601, Skalar) in the outlet tube.
The expected values of the wall shear stress are relatively low. A highly flexible gel layer is required to guarantee sufficiently large displacements. The gel, used in this study, was a 4 % solution of gelatin in water. The properties of the gel were measured with a parallel-plate

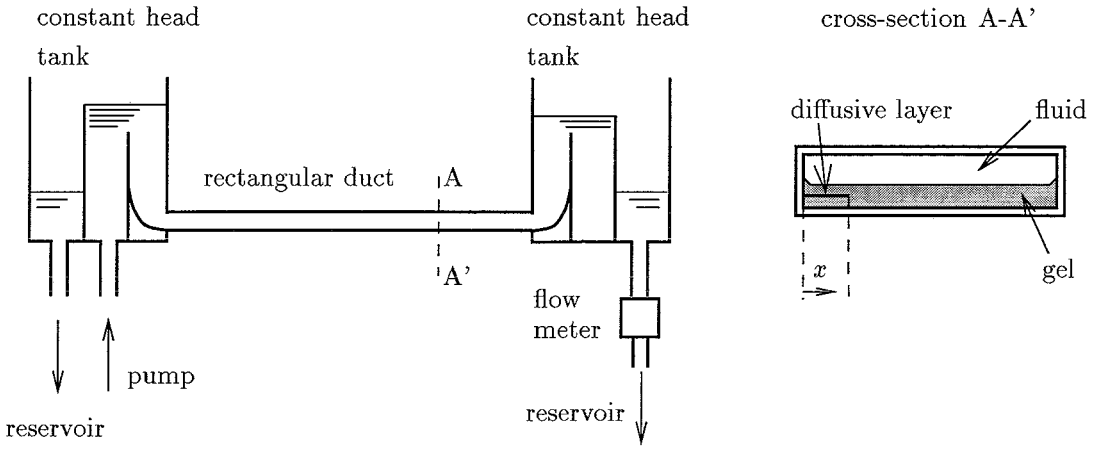

Figure 4.4: *Schematic presentation of the fluid circuit*

viscometer (RFSII, Rheometrics). The gel was essentially elastic with a bulk modulus of 500 Pa. Deformation measurements with SPI can only be performed if the laser beams are reflected by a diffusive surface. The natural surface of the gel layer is specular and a diffusive layer is necessary. A thin layer of titanium-oxide flakes (Iriodine, Merck) in the gel layer ($h = 1$ $[mm]$) provided provided a diffusive surface.

4.2.4 Experimental procedure

From the analytical solution of the velocity field in a rectangular duct (Ward-Smith (1980)), the velocity gradient along the gel layer was computed. The wall shear rate, multiplied by the dynamic viscosity of water, yields the theoretical wall shear stress. From the side wall, the wall shear stress will increase from zero at the side wall to its maximum value in the fully developed flow in the center of the duct. The wall shear stress induced deformation of the gel layer of an area 350 mm from the entrance of the duct was measured. The square area extended from $x = 0$ mm (side wall) to $x = 7$ mm (see also figure 4.4), and the deformation of the gel layer was measured for a range of flow rates.

4.3 Results

The deformation of the gel layer was measured for 7 different flow rates. For each flow rate, the measured speckle pattern was subtracted from the reference speckle pattern at zero flow. The resulting fringe pattern contained the displacement of the measured area. Since the flow was assumed to be fully developed and the gel layer to be homogeneous, the displacement of the gel layer was expected to be constant for constant x. The fringe distribution should therefore exhibit fringes parallel to the wall of the duct (figure 4.5). The intensity of the measured fringe pattern was averaged over an area Δy and the one dimensional fringe distribution was approximated by an absolute sine function (equation 4.4). A displacement $u(x)$ was chosen, resulting in a phase difference $\delta(x)$ and a first approximation for the one dimensional irradiance distribution $Ir(x)$. The difference between the measured and the fitted irradiance distribution was minimized, suing the least square method. The approximation procedure resulted in an optimal fitted irradiance distribution, that was converted to a fitted displacement through equation 4.3. The procedure is visualized in figure 4.5 for a flow rate of 1.11 l/min. On the left, the measured fringe pattern is depicted. The averaged and fitted mean irradiance and the resulting displacement are shown

on the right. For each flow rate, the measured fringe pattern was divided into 10 equal parts (Δy) and the fitting procedure was repeated for each Δy.

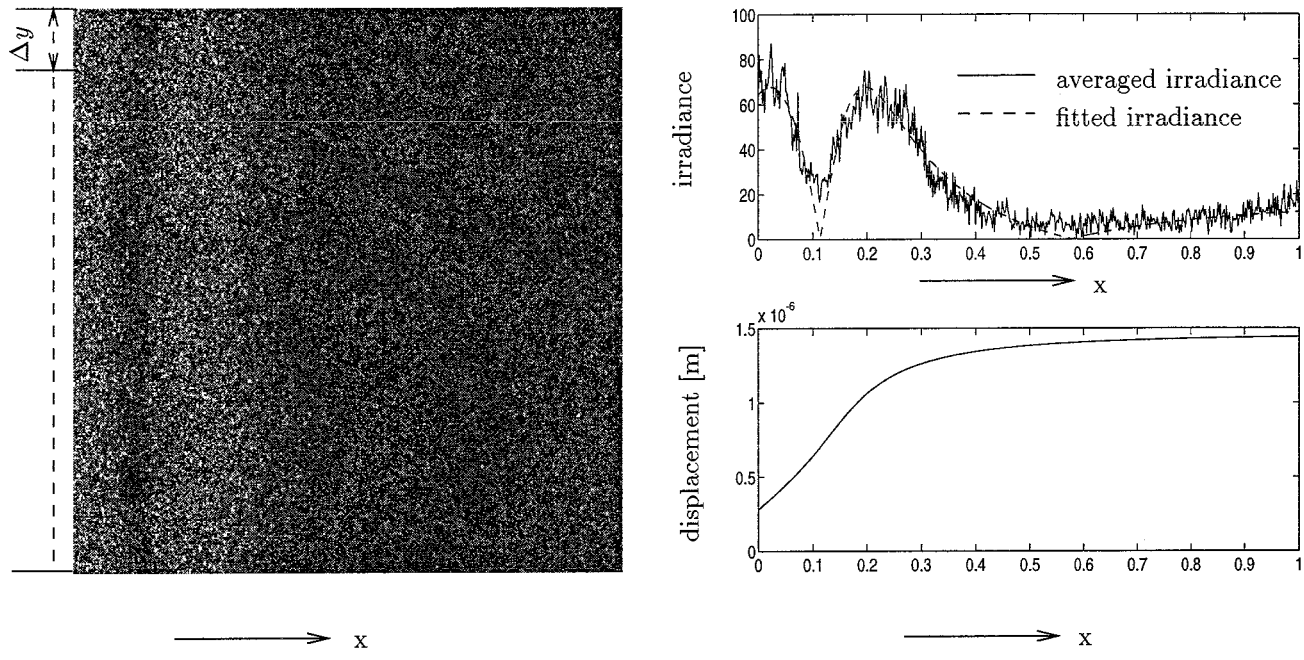

Figure 4.5: *Measured speckle pattern (left) and averaged and fitted irradiance and fitted displacement (right) for* $Q = 1.11\ l/min$

The expected fringe pattern, with the fringes parallel to the wall, can be discerned clearly. In the averaged fringe distribution, the position of the fringes can be seen readily. The fitting procedure yields a displacement distribution that is non-zero at the wall: this is caused by a displacement of the duct. This off-set of the displacement can be subtracted from the fitted displacement to yield the displacement of the gel layer.
The measured wall shear stress was inferred directly from the displacement through equation 4.1 and compared to the theoretical wall shear stress distribution for three flow rates (figure 4.6).
The measured values of the wall shear stress in fully developed flow show an excellent agreement with the theoretically imposed wall shear stress values. However, the measured wall shear stress distribution near the side wall is substantially lower than the expected wall shear stress. The gel layer clings to the side wall and the displacement of the gel layer will be lower due to the bending stiffness of the gel. Furthermore, the increased thickness of the gel layer near the side wall (see also figure 4.4) will influence the flow pattern and thus the expected wall shear stress distribution.
Finally, a comparison between the imposed and the measured wall shear stress in fully developed flow is presented in figure 4.7.
The measured wall shear stress shows an almost perfect linear fit (not shown), but the slope of the fitted line is not exactly equal to one, being 4% higher. This indicates that the estimated value of G/h is too high: either the thickness of the gel layer or the shear modulus of the gel were not determined accurately or altered during the measurements.

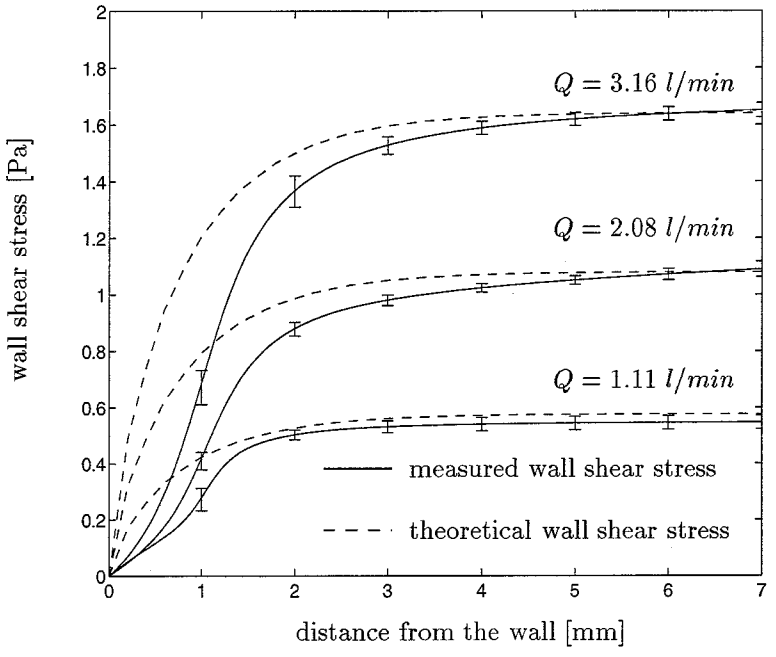

Figure 4.6: *Wall shear stress measurement in the boundary layer for three different flow rates*

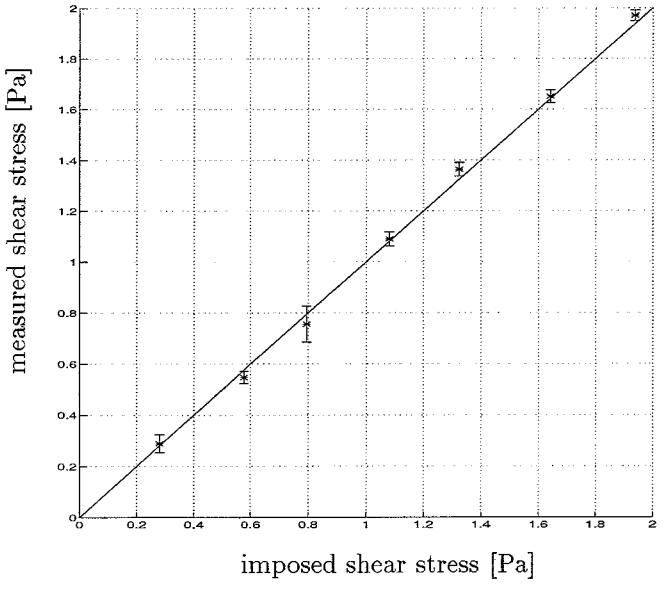

Figure 4.7: *Measured wall shear stress versus imposed wall shear stress in fully developed flow*

4.4 Discussion and conclusion

A new method to measure the wall shear stress was evaluated in a rectangular duct under steady flow conditions. The value of the wall shear stress was inferred from the deformation of an elastic gel layer inside the flow cell. The deformation of the gel layer was accurately measured by means of SPI and through the properties of the gel layer, the wall shear stress was computed. The measured wall shear stress in the fully developed flow showed an excellent agreement with the expected wall shear stress while the kinematic boundary conditions for the gel layer influenced its response near the side wall of the duct.

Three aspects determine the accuracy of the wall shear stress measurement: the displacement measurement, the properties of the gel layer, and the loading condition of the gel layer in the flow cell. The displacement measurements were performed with a relatively cheap and simple SPI apparatus. In a benchmark experiment, involving the measurement of the displacement of a carefully controlled rotating screw, an accuracy of 50 nm was achieved. Furthermore, the measurements are not disturbed by out-of-plane displacement of the gel layer, an advantage when measuring the wall shear stress in a parallel flow. The main drawback of the apparatus is its lack of directional sensitivity. A positive displacement yields exactly the same fringe pattern as an equally big negative displacement. Since the displacement of the gel layer in more complex flow can be both positive and negative, directional sensitivity would increase the applicability of the SPI apparatus. Several methods to include directional sensitivity are available and are currently assessed for future incorporation in the SPI apparatus. The properties of the gel layer, the shear modulus of the gel and the thickness of the layer, transfer the measured displacement to the wall shear stress. Both must be determined accurately and remain unaltered once placed in the flow model. Depending on the chemical composition of the fluid, the gel layer may swell or part of the solid fraction of the gel may dissolve in the fluid. The deviation of the fitted line in figure 4.7 can be attributed to the altered properties of the gel. Application of the method in more complex flows or fluids, should therefore be accompanied by a calibration procedure to determine the value of G/h *in-situ*. The third aspect that influences the measured displacement is the loading condition of the gel layer. Equation 4.1 is only valid for a freely moving gel layer subjected to a shear load. Both the dynamic and the kinematic boundary conditions for the gel layer can alter the response of the gel layer and equation 4.1 should be regarded with caution. A gradient in the wall shear stress, e.g. in the neighborhood of a stagnation point, results in a load on the gel layer that consists of both shear and tensile stress: equation 4.1 can not be applied. Equally important for the response of the gel layer are the kinematic boundary conditions, as can be concluded from figure 4.6. The gel layer clings to the side wall and the bending stiffness of the gel changes the response of the gel layer. Further research is required to investigate whether this aspect limits the applicability of this method.

With the current set-up, the wall shear stress in fully developed flow in a rectangular duct with a Newtonian fluid can be measured accurately. By replacing the Newtonian fluid by blood or a blood analog fluid, the influence of the non-Newtonian properties of these fluids on the wall shear stress can be investigated. Extension of this method to pulsatile flow requires directional sensitivity of the SPI apparatus and application in more complex geometries requires further research to assess the response of the gel layer.

Chapter 5

Conclusions and recommendations

5.1 Conclusions

Atherosclerosis develops preferentially in bends and bifurcations of the larger and medium sized arteries. The wall shear stress, exerted by the blood flow, is believed to play a pivoting role in the development of the atherosclerotic lesions. The wall shear stress is defined as the product of the wall shear rate and the viscosity of blood. *In-vitro* experiments under physiologically relevant flow conditions are relevant to transfer *in-vivo* blood flow measurements to wall shear stress distributions.

The viscosity of blood is shear rate and erythrocyte concentration dependent. In viscometric studies, the shear stress can be measured as a function of the shear rate and erythrocyte concentration. Blood exhibits non-homogeneous shear rate and concentration distributions, even in simple shear flow. The measured shear stresses in simple shear flow, the prevailing flow condition at near wall sites, can only be transferred to physiologically relevant flow conditions if the shear rate and the concentration distributions are comparable.

The non-Newtonian properties of blood are believed to be relatively insignificant in the larger arteries. However, LDA experiments in a three dimensional model of the carotid bifurcation, using a shear thinning, viscoelastic blood analog fluid, showed that the steady flow patterns altered significantly due to the non-Newtonian fluid properties. Both large scale flow phenomena and near wall velocity distributions changed, mainly due to the viscoelasticity of the blood analog fluid. The wall shear rate estimations from the LDA experiments showed that in the carotid sinus near the non-divider wall, the preferred site for the development of atherosclerotic lesions, the wall shear rate was always positive for the blood analog fluid while negative wall shear rates were found for the Newtonian fluid. It should be noted however, that the extrapolation method for the wall shear rate was rather inaccurate and highly sensitive for the estimated position of the wall. Any investigation, dealing with the wall shear stress distribution in the larger arteries, must include not only the particulate nature of blood but also the appropriate non-Newtonian properties.

The complexity of blood poses major difficulties in determining its near wall viscosity. Instead of focusing on the fluid, the response of a gel layer, attached to the inner wall of a rectangular duct, was used to evaluate the wall shear stress. Speckle pattern interferometry was applied to measure the response of a highly flexible, elastic gel layer under steady flow conditions. In a physiologically relevant range, the wall shear stress was measured accurately for a Newtonian fluid, indicating that this method can be used to evaluate the influence of non-Newtonian fluid properties on the wall shear stress in a simple two dimensional flow. If directional sensitivity of the SPI apparatus is incorporated and if the behavior of the gel layer can be described properly, this method can be used in complex geometries under pulsatile flow conditions.

5.2 Recommendations

From the LDA experiments in the carotid bifurcation, it is obvious that a proper blood analog fluid is indispensable. The microscopic structure of the KSCN-Xanthan-gum solution used for the LDA experiments is not comparable to the particulate nature of blood and prevents a complete match to the non-Newtonian properties of blood. The blood analog fluid for future experiments should therefore have a microscopic structure, comparable to blood, and should be optically transparent. A concentrated suspension of ghost cells offers the best prospects. If a fluorescent dye is enclosed in a fraction of the ghost cells, fluorescence microscopy can be applied to perform particle tracking velocimetry (PVT). PVT can be used to investigate near wall velocity and concentration distributions.
The behavior of the ghost cell suspension will be investigated in simple shear flow. A viscometer will be adapted to enable florescence microscopy and to simultaneously measure the wall shear stress. The numerical modelling of the suspension flow involves solving a highly non-linear convection-diffusion equation to compute the concentration distribution of the particles. This concentration distribution serves as a parameter for a relatively simple constitutive equation. The Navier-Stokes equations can then be solved. The computed wall shear stress, velocity and concentration distributions can be compared to the experimental data and the model for the suspension flow can be assessed.
The next step involves investigation of two dimensional flows. The two dimensional flow experiments will involve Poiseuille flow and flow behind a step. PTV will be combined with the new method to measure the wall shear stress with SPI. Comparison of the numerical and measured data can be used check the validity of the numerical model for two dimensional flows. Finally, the wall shear stress and velocity and concentration distributions in a rigid bend, using the ghost cell suspension as the measuring fluid, will be investigated.

Bibliography

Aarts, P., Steendijk, P., Sixma, J., and Heethaar, R. (1986). Fluid shear as a possible mechanism for platelet diffusivity in flowing blood. *J. Biomechanics*, **19**, 799–805.

Baaijens, J., van Steenhoven, A., and Janssen, J. (1993). Numerical analysis of steady generalized newtonian flow in a 2d model of the carotid artery bifurcation. *Biorheology*, **30**, 63–74.

Ballyk, P., Steinman, D., and Ethier, C. (1994). Simulation of non-newtonian blood flow in an end-to-side anastomosis. *Biorheology*, **31**, 565–586.

Bharadvaj, B., Mabon, R., and Giddens, D. (1982). Steady flow in a model of the human carotid bifurcation. part II: Laser-doppler measurements. *J. Biomechanics*, **15**, 363–378.

Bugliarello, G. and Sevilla, J. (1970). Velocity distribution and other characteristics of steady and pulsatile blood flow in fine glass tubes. *Biorheology*, **7**, 85–107.

Burton, A. (1965). *Physiology and Biophysics of the Circulation*. Year Book Medical Publishers inc.

Caro, C., Fitzgerald, J., and Schroter, R. (1971). Atheroma and arterial wall shear: Observation, correlation and proposal of a shear dependent mass transfer mechanism for atherogenesis. *Proc. Roy. Soc. London, B*, **177**, 109–159.

Caro, C., Pedley, T., and Schroter, R. (1978). *Mechanics of the Circulation*. Oxford University Press.

Chien, S. (1979). *Blood Rheology*, chapter 6. In Hwang *et al.* (1979).

Chien, S., Usami, S., Dellenback, R., and Gregersen, M. (1969). Shear-dependent deformation of erythrocytes in rheology of human blood. *American Journal of Physiology*, **219**, 136–142.

Cokelet, G. (1972). *The Rheology of Human Blood*, chapter 4. In Fung *et al.* (1972).

Cokelet, G. and Goldsmith, H. (1991). Decreased hydrodynamic resistance in the two-phase flow of blood through small vertical tubes at low flow rates. *Circulation Research*, **68**, 1–16.

Copley, A., editor (1968). *Hemorheology*. Pergamon Press.

Erf, R., editor (1978). *Speckle Metrology*. Academic Press.

Fung, Y. (1993). *Biomechanics: mechanical properties of living tissues*. Springer-Verlag, 2nd edition.

Fung, Y., Perrone, N., and Anliker, M., editors (1972). *Biomechanics: its Foundations and Objectives*. Prentice Hall.

Giddens, G., Zarins, C., and Glagov, S. (1990). Response of arteries to near-wall fluid dynamic behavior. *Applied Mechanical Review*, **43**, S98–S102.

Goldsmith, H. (1993). Poiseuille medal award lecture: From papermaking fibers to human blood cells. *Biorheology*, **30**, 165–190.

Goldsmith, H. and Marlow, J. (1979). Flow behaviour of erythrocytes. II: Particle motions in concentrated suspensions of ghost cells. *J. of Colloid and Interface Science*, **71**, 383–407.

Goldstein, R., editor (1983). *Fluid Mechanics Measurements*. Hemisphere Publishing Company.

Hanratty, T. and Campbell, J. (1983). *Measurement of wall shear stress*, chapter 11. In Goldstein (1983).

Hwang, N., Gross, D., and Patel, D., editors (1979). *Quantative Cardiovascular Studies*. University Park Press.

Jones, R. and Wykes, C., editors (1989). *Holographic and Speckle Interferometry*. Cambridge University Press.

Karino, T. and Goldsmith, H. (1979). Aggregation of platelets in an annular vortex distal to a tubular expansion. *Microvascular Research*, **17**, 217–237.

Karnis, A., Goldsmith, H., and Mason, S. (1966). The kinetics of flowing dispersions. I: concentrated suspensions of rigid particles. *J. of Colloid and Interface Science*, **22**, 531–553.

Ku, D. and Giddens, D. (1987). Laser doppler measurements of pulsatile flow in a model carotid bifurcation. *J. Biomechanics*, **20**, 407–421.

Ku, D. and Liepsch, D. (1986). The effect of non-newtonian viscoelasticity and wall elasticity on flow at a 90 degree bifurcation. *Biorheology*, **23**, 359–370.

Liepsch, D. and Moravec, S. (1984). Pulsatile flow of non-newtonian fluid in distensible models of human arteries. *Biorheology*, **21**, 571–586.

Mann, D. and Tarbell, J. (1990). Flow of non-newtonian blood analog fluids in rigid curved and straight artery models. *Biorheology*, **27**, 711–733.

McMillan, D., Strigberger, J., and Utterback, N. (1987). Rapidly recovered transient flow resistance: a newly discovered property of blood. *Am. J. Physiol.*, **253**, 919–926.

Merrill, E. (1969). Rheology of blood. *Physiological Reviews*, **49**, 863–888.

Nerem, R. (1992). Vascular fluid mechanics, the arterial wall, and atherosclerosis. *Journal of Biomechanical Engineering*, **114**, 274–282.

Palmen, D. (1994). *The influence of minor stenoses on carotid artery flow*. Ph.D. thesis, Eindhoven University of Technology.

Perktold, K., Peter, R., Resch, M., and Langs, G. (1991). Pulsatile non-newtonian flow in three-dimensional carotid bifurcation models: a numerical study of flow phenomena under different bifurcation angles. *J. Biomed. Eng.*, **13**, 507–515.

Phibbs, R. (1968). *Orientation and distribution of erythrocytes in blood flowing in medium-sized arteries.*, pages 617–630. In Copley (1968).

Philips, R., Armstrong, R., Brown, R., Graham, A., and Abbott, J. (1992). A constitutive equation for concentrated suspensions that accounts for shear-induced particle migration. *Phys. Fluids*, 4, 30–40.

Rindt, C., van Steenhoven, A., Janssen, J., Reneman, R., and Segal, A. (1990). A numerical analysis 6of steady flow in a three-dimensional model of the carotid artery bifurcation. *J. Biomechanics*, **23**, 461–473.

Schmid-Schönbein, H., Wells, R., and Goldstone, J. (1971). Fluid drop-like behavior of erythrocytes- disturbance in pathology and its quantification. *Biorheology*, **7**, 227–234.

Tangelder, G., Slaaf, D., Muijtjens, A., Arts, T., oude Egbrink, M., and Reneman, R. (1986). Velocity profiles of blood platelets and red blood cells flowing in arterioles of the rabbit mesentry. *Circulation Research*, **59**, 505–514.

Tanner, L. and Blows, L. (1976). A study of the motion of oil films on surfaces in air flow, with application to the measurement of skin friction. *Journal of Physics E.*, **9**, 194–202.

Thurston, G. (1973). Frequency and shear rate dependence of viscoelasticity of human blood. *Biorheology*, **10**, 375–381.

Wang, S. and Hwang, N. (1992). On transport of suspended particles in tube flow. *Biorheology*, **29**, 353–377.

Ward-Smith, A. (1980). *Internal fluid flow*. Clarendon Press.

Winter, K. (1977). An outline of the techniques available for the measurement of skin friction. *Prog. Aerosp. Sci.*, **18**, 1–57.

Woldhuis, B. (1993). *Blood platelet rheology in venules and arterioles.* Ph.D. thesis, Limburg University, Maastricht.